

**KERNFORSCHUNGSZENTRUM  
KARLSRUHE**

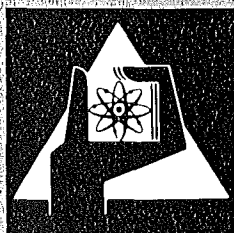
Dezember 1977

KFK 2545

Institut für Reaktorbauelemente  
Projekt Nukleare Sicherheit

**An Analytical Study of the Thermo-Hydrodynamic  
Behavior of the Reflood-Phase During a LOCA**

Y. Murao



**GESELLSCHAFT  
FÜR  
KERNFORSCHUNG M.B.H.**

**KARLSRUHE**

Als Manuskript vervielfältigt

Für diesen Bericht behalten wir uns alle Rechte vor

GESELLSCHAFT FÜR KERNFORSCHUNG M. B. H.  
KARLSRUHE

KERNFORSCHUNGSZENTRUM KARLSRUHE

KFK 2545

Institut für Reaktorbauelemente

Projekt Nukleare Sicherheit

AN ANALYTICAL STUDY OF THE THERMO-HYDRODYNAMIC  
BEHAVIOR OF THE REFLOOD-PHASE DURING A LOCA

Y. Murao

GESELLSCHAFT FÜR KERNFORSCHUNG MBH, KARLSRUHE



AN ANALYTICAL STUDY OF THE THERMO-HYDRODYNAMIC  
BEHAVIOR OF THE REFLOOD-PHASE DURING A LOCA

---

Yoshio Murao\*

ABSTRACT

The objectives of this study are

- the check of the quench model proposed by the author and T. Sudoh,
- the establishment of the thermo-hydrodynamics downstream from the quench front, and
- the stabilization of the numerical calculations.

In order to study these terms, the new version of the reflow analysis code "REFLA-1D" was developed.

The quench modes were classified into the following three types:

- 1.) Liquid column type (rewetting by subcooled water),
- 2.) Dryout type (annular flow type, rewetting by saturated water), and
- 3.) Rewetting type (entire surface temperature higher than rewetting temperature).

For the thermo-hydrodynamic model downstream from the quench front, the flow pattern was divided into the five regimes:

- 1.) Subcooled film boiling regime,
- 2.) Transition flow regime,
- 3.) Dispersed flow regime,
- 4.) Superheated steam flow regime, and
- 5.) Rewetted regime.

To stabilize the numerical calculation and shorten the computing time, the Lagrangian form of the energy equation of gas phase and dispersed flow region was used instead of the Eulerian form.

Considerably close agreement between three PWR-FLECHT tests and the calculated results for the critical Weber number  $We_c = 1.0$  was obtained for fuel clad surface temperature and quench time except in earlier stage before turnaround, but poor agreement for the heat transfer characteristics in the transition flow region defined between the quench front and the dispersed flow region.

The calculation was relatively stable and the computing time is about the same as a real time for a IBM 370-158 computer.

---

\* Assigned to Gesellschaft für Kernforschung mbH., Postfach 3640, 7500 Karlsruhe 1, Federal Republic of Germany from Japan Atomic Energy Research Institute, Tokai-mura, Naka-gun, Ibaraki-ken, Japan  
14th July 1975 - 6th July 1976

Eine analytische Studie über das thermohydraulische Verhalten der Flutphase während eines LOCA

---

Yoshio Murao\*

Kurzfassung

Die Ziele dieser Untersuchung sind:

- die Überprüfung des Benetzungsmodells, das von dem Autor und T. Sudoh vorgeschlagen wurde,
- die Beschreibung der Thermo- und Hydrodynamik strömungsabwärts von der Benetzungsfront und
- die Stabilisierung der numerischen Berechnung.

Zur Untersuchung dieser Probleme wurde die neue Version des Rechenprogrammes REFLA-1D zur Analyse der Flutphase entwickelt.

Bezüglich des Benetzungsvorganges wurde unterschieden zwischen den folgenden Typen:

- 1.) Benetzung durch unterkühltes Wasser,
- 2.) Benetzung durch gesättigtes Wasser und
- 3.) Temperatur der gesamten Staboberfläche oberhalb der Benetzungstemperatur.

Für das thermohydraulische Modell strömungsabwärts von der Benetzungsfront wurde die Strömung aufgegliedert in fünf Bereiche:

- 1.) den Bereich mit unterkühltem Filmsieden,
- 2.) den Übergangsbereich,
- 3.) den Bereich mit Nebelströmung,
- 4.) den Bereich mit überhitztem Dampf und
- 5.) den wiederbenetzten Bereich.

Zur Stabilisierung der numerischen Berechnung und zur Reduzierung der Rechenzeit wurde anstelle der Euler'schen die Lagrange'sche Form der Energiegleichung für die Strömungsbereiche des einphasigen Dampfes und des Flüssigkeitnebels verwendet.

Für die kritische Weber-Zahl  $We_c = 1.0$  ergibt sich beim Vergleich von drei PWR-FLECHT Experimenten mit den Rechenergebnissen eine bemerkenswert gute Übereinstimmung der Staboberflächen-temperatur und der Benetzungszeit mit Ausnahme der Zeit bis zum Absinken der Hüllrohrtemperatur. Schlecht ist dagegen die Übereinstimmung des charakteristischen Wärmeübergangs im Übergangsbereich zwischen der Benetzungsfront und der Nebelströmung.

Die Rechnung war relativ stabil. Die Rechenzeit entspricht ungefähr der Problemzeit bei Verwendung einer Computeranlage vom Typ IBM 370-158.

---

\* Delegiert zur Gesellschaft für Kernforschung mbH., Postfach 3640, 7500 Karlsruhe 1, Bundesrepublik Deutschland vom Japan Atomic Energy Research Institute, Tokai-mura, Naka-gun, Ibaraki-ken, Japan in der Zeit vom 14. Juli 1975 bis zum 6. Juli 1976.



## TABLE OF CONTENTS

### ABSTRACT

1. INTRODUCTION
  
2. PRELIMINARY DISCUSSION OF THE REFLOOD MODEL
  - 2.1 Flow models
  - 2.2 Quench models
  - 2.3 Thermo-hydrodynamics in the quenched region
  - 2.4 Thermo-hydrodynamics in the unwetting two-phase flow
  - 2.5 Summary of this chapter
  
3. MATHEMATICAL EXPRESSION OF THE PROBLEM
  - 3.1 Basic thermo-hydrodynamic equations for coolant in the quenched region and superheated steam flow region
  - 3.2 Basic thermo-hydrodynamic equations for coolant in the unwetting two-phase flow
  - 3.3 Thermal equations on the fuel rod
  
4. NUMERICAL CALCULATION
  - 4.1 Calculation method for dispersed flow
  - 4.2 Calculation method for energy equation of liquid phase flow and superheated steam flow
  - 4.3 General calculation method
  - 4.4 Transition from the forced convection heat transfer to the boiling heat transfer
  - 4.5 Structure of the computer program
  - 4.6 Power distribution and decay heat curve
  - 4.7 Control sequence of the calculation
  - 4.8 Logics for determining the boundaries of the regions
  - 4.9 Form of the input data
  - 4.10 Stored output data
  - 4.11 Sample input data

- 5. RESULTS AND DISCUSSION
  - 5.1 Temperature histories
  - 5.2 Effects of critical Weber number
  - 5.3 Check of quench model
  - 5.4 Numerical calculation

6. CONCLUSION

ACKNOWLEDGEMENT

REFERENCES

NOMENCLATURE

## 1. INTRODUCTION

In the safety analysis on the Loss-of-Coolant Accident (LOCA) of Light Water Reactors, it is very important to evaluate the temperature history of the fuel rod claddings during the reflood phase, which is governing the integrity of the first enclosure of the fission products.

Thought the reflood phase is affected by so-called system effects (steam binding, downcomer, hot wall effect and so on) and flow redistributions caused by fuel deformation, as a first stage, we intended to develop a thermo-hydrodynamic analysis code for a single coolant channel in a reactor core without system effects and with coolant injection at a constant flow rate.

The computer code is thought to be the basis for the extension to an integrated reflood phase analysis code. Even though the thermo-hydrodynamic behavior in the reactor core contains some uncertified phenomena, e.g. so-called quench phenomena and thermo-hydrodynamics of "unwetting" two-phase flow which cannot wet the channel wall due to so-called "Leidenfrost phenomenon", but if we try to repeat modifications of the computer code by checking the inconsistency of the code itself and comparing the calculated results with experimental data, we will get a more realistic reflood model on thermo-hydrodynamics in the reactor core.

Based on this philosophy, the first version of the reflood analysis code "REFLA-1" was developed and it revealed the following problems<sup>(1)</sup>.

- 1.) The quench model used in the code was not suitable. As a quench model, an one-dimensional heat conduction model was adopted, which was similar to Yamanouchi's model<sup>(2)</sup> but used more sophisticated heat transfer characteristics like

a boiling curve instead of a step-wise function.

The standard boiling curve did not give a proper quench velocity and the modification of "boiling curve" was tried. It was found that the maximum heat flux, the minimum wall superheat, and the transition boiling correlation should be determined but that was difficult because only few informations are given by experimental data.

- 2.) The film boiling correlation predicted a higher heat transfer coefficient near the quench front than the measured value. Downstream from the quench front, the liquid column region was assumed to be existing and the Ellion's film boiling correlation applicable. The Ellion's correlation <sup>(3)</sup> indicates that the heat transfer coefficient is inversely proportional to a fourth power of linear dimension assumed as a distance from the quench front. And so that gave very large value near the quench front.
- 3.) The single gas-phase correlation gave lower heat transfer coefficients than the measured values and caused the instability of numerical calculations. Downstream from the liquid column region, the dispersed flow and the superheated steam regions were assumed to be existing and the single gas-phase correlation applicable. In dispersed flow region, it was found that the effect of droplets on the heat transfer could not be neglected.

The calculated vapor velocity was too high to use a large time step which was necessary for calculations of the re-flood phase, i.e. the time period of re-flood phase was of an order of two to four hundred seconds.

According to the text book on numerical calculations<sup>(4)</sup>, the time step has to be smaller than the convection time in usual calculation method.

Another effect was a rapid temperature rise of the vapor due to small heat capacity. That caused a rapid decrease of the heat transfer to the vapor and therefore the temperature of vapor fell down rapidly. Such an interaction resulted instabilities in the thermo-hydrodynamic calculation of the single gas-phase flow.

- 4.) It was concluded that the liquid column region might disappear under the saturated condition at the quench front. Because, if the water is saturated at the quench front, the flow at the quench front becomes an annular two-phase flow due to the high heat transfer rate near the quench front and the generated vapor blows up the liquid column. And so the liquid column region was considered to be existing under the liquid subcooled condition.

Based on the results mentioned above, some experiments and analysis were done in Japan Atomic Energy Research Institute. The author and Sudoh<sup>(5)</sup> proposed a new quench model, in which a quench velocity correlation was used instead of the heat conduction model and three different types of quench models were included. Sudo<sup>(6)</sup> developed the subcooled film boiling correlation empirically.

The objectives of this study are 1) the check of the quench model proposed by the author and Sudoh, 2) the establishment of the thermo-hydrodynamics downstream from the quench front, and 3) the stabilization of the numerical calculations. In order to study these items, the new version of the reflood analysis code, "REFLA-1D", was developed.

In this code, the following extreme case was considered in regard to the release of the stored energy from a fuel rod to simplify the calculation:

(1) Most of the stored energy,  $C_{pF} \cdot \gamma_F \cdot (T_w - T_s - 50.0)$ , is released at the quench front and the rest of the stored energy is gradually released when the wall temperature falls down.

(2) The radial temperature profile of a fuel rod is flat.

## 2. PRELIMINARY DISCUSSION OF REFLOOD MODEL

### 2.1. Flow models

The following flow patterns shown in Fig. 2.1 have been observed in the heated quartz (transparent) tube by injecting water into the tube<sup>(5)</sup>.

As expected from the results of the "REFLA-1" code <sup>(1)</sup>, under the subcooled condition at the quench front it was found a) the water could wet the heated tube wall upstream from the quench front, b) the water could not wet the wall downstream from the quench front and a liquid column was formed in the center of the coolant channel, and c) when the length of the liquid column reached a certain value, the excess water was separated into large droplets at the top of the liquid column and these droplets flew to the top of the tube.

Under saturation condition at the quench front, as expected from the "REFLA-1" code, d) an annular flow region was formed upstream from the quench front and sometimes the excess water was formed like bridge at the top of annular flow and was blown up by the vapor upstream from the quench front. And so, a liquid column did not appear downstream from the quench front. The excess water was turned into some droplets and flew up to the top of the tube.

When the wall temperature fell down to a critical temperature, the water began to wet the tube wall, i.e. rewetting occurred. Such a rewetting was observed under the both conditions.

Similar flow patterns were described in the PWR-FLECHT report<sup>(7)</sup> as follows (Refer to Fig. 2-2):

"A stable film boiling regime existed just above the quench front or at the leading-edge of the transition boiling regime. The flow

pattern observed in the movies consisted of a thin vapor annulus around the rod surrounded by a continuous liquid phase.

The relatively low void fraction and the uniform appearance of the vapor layer suggested that the liquid was subcooled. (The local coolant thermocouple data also indicated the presence of subcooled liquid above the quench front).

Under other conditions, for example low flooding rates and high elevations, calculations indicated that the liquid above the quench front was at the saturation temperature. Just as an unstable transition regime existed between the nucleate and stable film boiling regime, an unstable flow pattern transition regime existed between the stable film boiling and dispersed flow regimes. In the flow pattern transition regime, the flow changed from mostly liquid, or the continuous liquid phase with vapor film boiling, to mostly steam, or the continuous vapor phase with dispersed droplet flow. ...."

Schmidt<sup>(8)</sup> observed the dispersed flow under the simulated reflood condition using nanosecond flash light and concluded that the diameter of droplets was about 0.5 millimeter but larger droplets were observed just after the start of the water injection. The droplet size observed by the author and Sudoh was about 2 to 3 millimeter and different from the size observed by Schmidt. It can be assumed that the initial diameter of the droplets is 2 or 3 millimeter and they are divided into finer droplets. The transition flow observed in PWR-FLECHT experiments<sup>(7)</sup> was not observed in the experiment by the author and Sudoh which was carried out under relatively low flow rate conditions.

It was also assumed that the water cannot fly in the vapor flow before a certain condition is satisfied, such a region is a transition flow region and the water stays in this region, i.e. the transition flow region is at the saturation temperature and does not satisfy a certain condition.



In the author and Sudoh's experiment, it was considered that the vapor was generated at a high rate and a certain condition was satisfied for a short length just after the liquid column region because of low flow rate condition. It was considered that the transition flow region might exist between the liquid column region and the dispersed flow region or between the quench front with local saturation temperature and the dispersed flow region under the normal reflood conditions.

According to the PWR-FLECHT report<sup>(7)</sup>, the flow pattern was corresponding to the heat transfer as follows. (Refer to Fig. 2-3).

The first peak of the heat transfer coefficient curve corresponded to the start of the transition flow regime (end of dispersed flow) and the last valley corresponded to the start of the film boiling regime (end of transition flow regime).

The start of the dispersed flow regime (end of steam flow) was interpreted to be the point at which the heat transfer coefficient first began to rise rapidly.

According to the author and Sudoh's analysis<sup>(5)</sup> on PWR-FLECHT report, most of the heat transfer coefficient curves were classified into the following two groups (Refer to Fig. 2-4).

The group 1 has a middle steep range A, but the group 2 does not have such a middle steep range. The group 1 appears under the subcooled condition at the quench front. And so, it can be estimate that the range A is corresponding to subcooled film boiling region.

An unique relation seems to exist between the flow pattern and the heat transfer and the flow pattern seems to be classified two types, i.e. one type corresponds to the subcooled condition at the quench front and an another type corresponds to the saturated condition at the quench front.

Based on the discussion above the following flow model shown in Fig. 2-5 was assumed as a reflow flow model. The type 1 flow pattern appears under the subcooled condition at the quench front. Upstream from the quench front, the injected water enters the liquid phase region and subcooled nucleate boiling region. Downstream from the quench front, the water enters the subcooled film region (the water temperature is lower than saturation temperature), the transition flow region (the water is at the saturation temperature and the criterion for transition is not satisfied), the dispersed flow region (the criterion is satisfied and droplets are formed and accelerated), the rewetted region (when the wall temperature is lower than a critical temperature) and the superheated steam flow region (only when the water does not exist in the region).

The type 2 flow pattern appears under the saturated condition at the quench front. The flow pattern is nearly the same as the type 2 flow pattern but except the regions near the quench front. The saturated two-phase flow appears upstream from the quench front and the subcooled film boiling region does not appear downstream from the quench front.

In the regions between the quench front and the rewetted region, the water does not wet the heating wall and these regions will be defined as an "unwetting two-phase flow" region.

The regions which have already been wetted by the water will be defined as "quenched" regions.

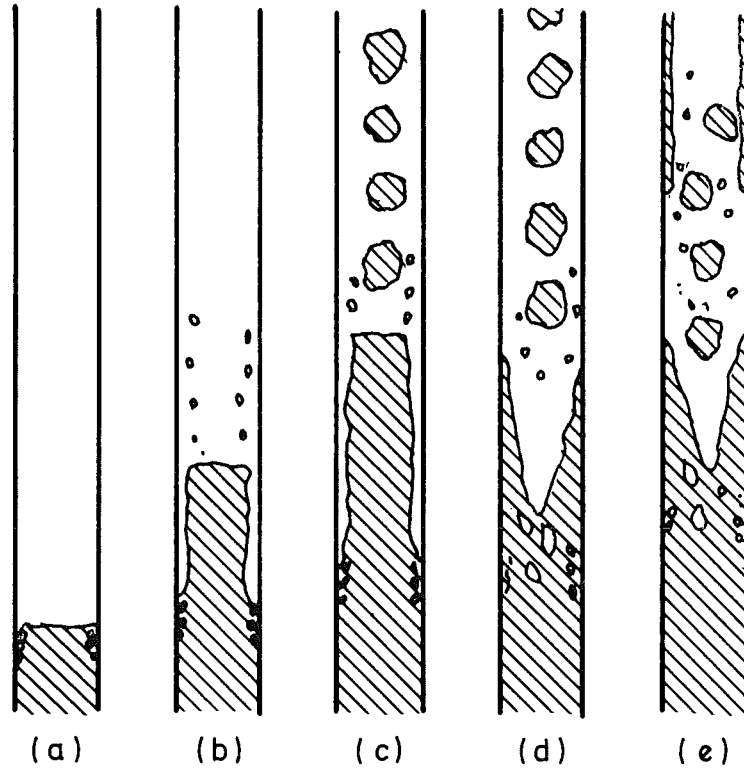


Fig. 2-1

Models of Flow Pattern

( Taken from Reference (5) )

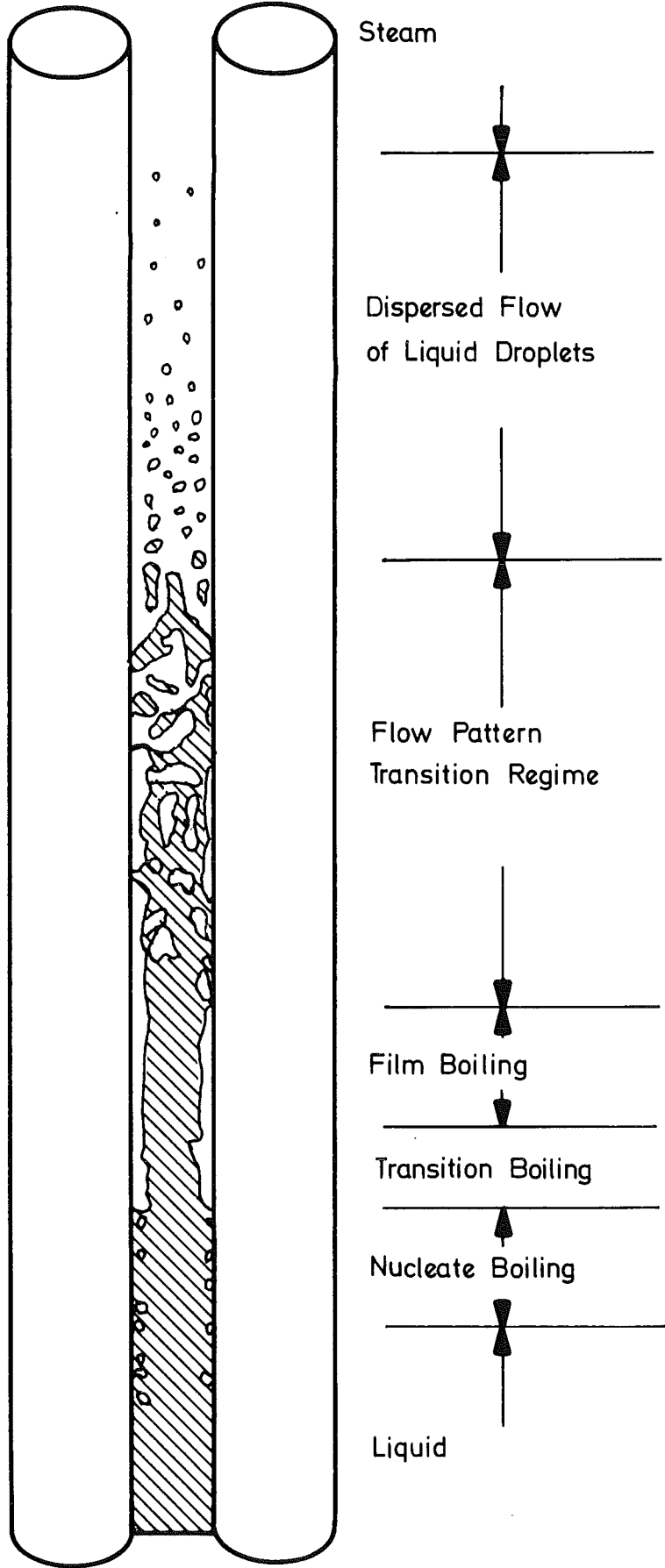


Fig. 2-2

FLECHT Flow Regimes

(Taken from Reference (7))

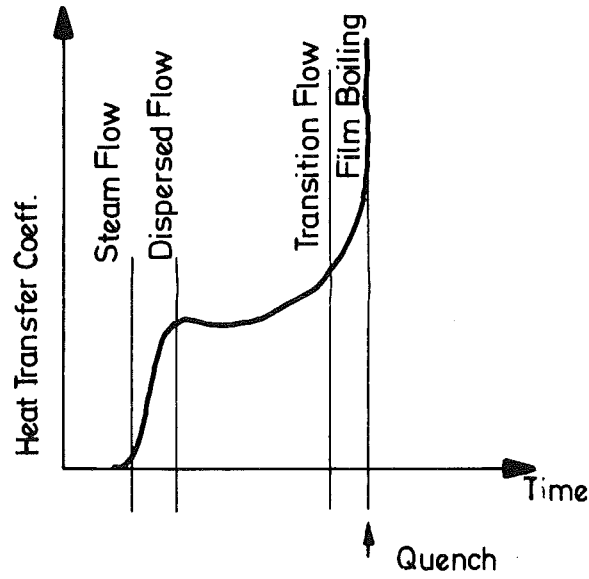


Fig 2-3 Typical Heat Transfer Behavior  
( Taken from Reference (7) )

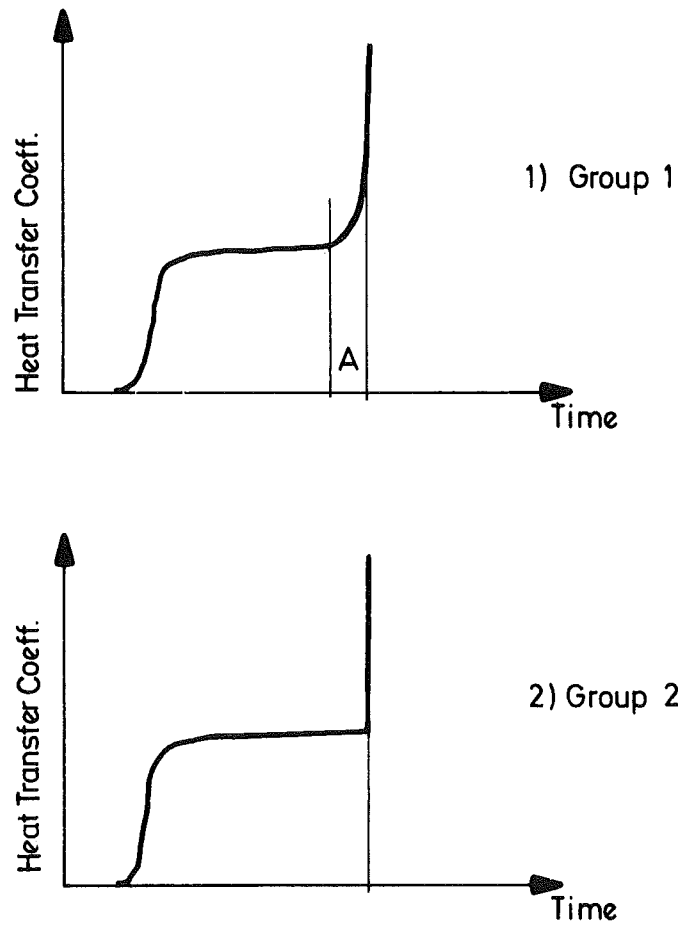


Fig. 2-4 Two Types of the Heat Transfer Behavior  
( Taken from Reference (5) )

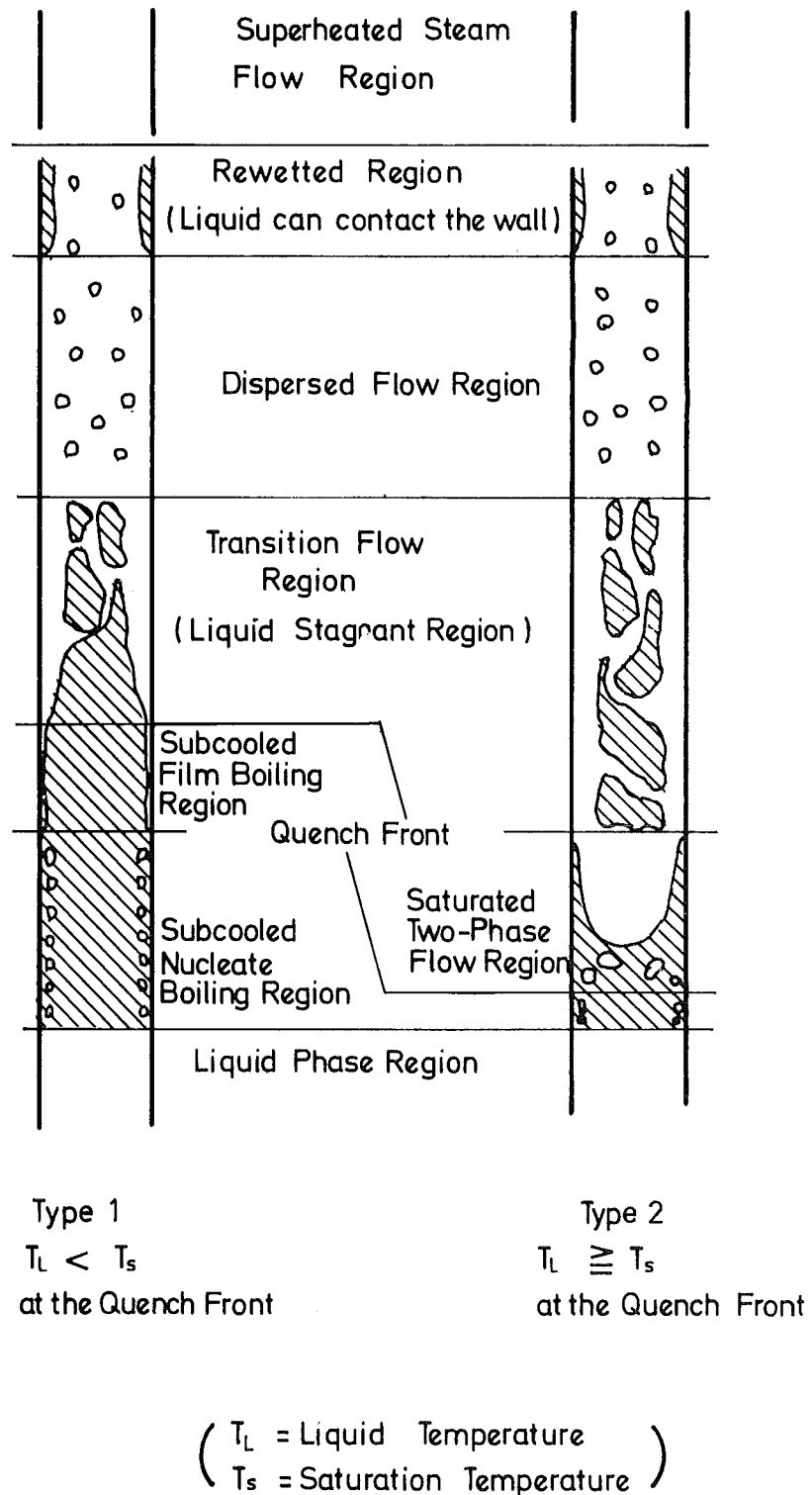


Fig. 2 - 5

Two Types of the Flow Pattern During Reflood Phase

## 2.2 Quench models

Based on the flow pattern observed in the outside-heated quartz tube, the author and Sudoh<sup>(5)</sup> proposed the following quench models shown in Fig. 2-6. The quench models can be classified into three types, i.e.

- 1) Liquid column type (rewetting by subcooled water)
- 2) Dryout type (Annular flow type ,rewetting by saturated water)
- 3) Rewetting type (entire surface temperature higher than re-wetting temperature)

In the first and second types, there are a quenched part and non-quenched part and these are divided by the so-called quench front. From the non-quenched part to the quenched part, the heat is transferred by axial heat conduction and hence the quench front is advancing.

But in the third type, there is no quenched part and the quench phenomenon starts without the support of a quenched part. After the quench starts, the third type succeeds to the first or second one.

The first type occurs under the liquid subcooled condition and the second type occurs under the liquid saturated condition.

The critical temperature for the quench was assumed to be the maximum liquid superheat, above which the liquid phase cannot exist thermodynamically. The maximum liquid superheat was calculated by Groeneveld<sup>(9)</sup> using the Jusa's semiempirical equation of state which can be approximately expressed as follows

$$T_M = 321.05 \cdot 0.237 \cdot 10^{-4} p \quad (2.1)$$

where  $p$  is the pressure ( $\text{kg/m}^2$ )<sub>a</sub> and  $T_M$  is the maximum liquid superheat ( $^{\circ}\text{C}$ ).

Blair<sup>(10)</sup> derived the following correlation of quench velocity based on the theoretical analysis of the axial heat conduction problem.

$$U_q^{-1} = \rho_w \cdot g \cdot c_{pw} \cdot (T_w - T_o) / \phi_{eff} \quad (\text{h/m}) \quad (2.2)$$

where  $T_o$  is a critical temperature like a Leidenfrost temperature and  $\phi_{eff}$  is an effective axial heat flux which corresponds to a heat flux from the wall to the coolant just downstream from quench front,  $\phi$ , i.e.

$$\phi / \phi_{eff} = \frac{\pi}{2} \quad (2.3)$$

The author and Sudoh assumed that the critical temperature  $T_o$  is the maximum liquid superheat  $T_M$  and the heat flux  $\phi$  is a function of the liquid subcooling and the maximum heat flux  $\phi_{MAX}$ .

The following correlations of quench velocity were obtained by determining the effective heat flux  $\phi_{eff}$  from the data of Westinghouse's PWR-FLECHT experiment.

1) For the dryout type quench

$$U_q^{-1} = \rho_w \cdot g \cdot c_{pw} \cdot (T_w - T_o) / 2.19 \cdot 10^6 \quad (\text{h/m}) \quad (2.4)$$

and

$$\phi_{MAX} = 3.43 \cdot 10^6 \quad (\text{kcal/m}^2\text{h}) \quad (2.5)$$

2) For the liquid column type quench

$$U_q^{-1} = \rho_w \cdot g \cdot c_{pw} \cdot (T_w - T_o) / \{2.19 \cdot 10^6 \cdot (1 + 0.2778 \cdot 10^{-4} \cdot \Delta T_{sub}^3)\}$$

(h/m) (2.6) and

$$\phi_{MAX} = 3.43 \cdot 10^6 \cdot (1 + 0.2778 \cdot 10^{-4} \cdot \Delta T_{sub}^3) \quad (\text{kcal/m}^2\text{h}) \quad (2.7)$$



3) For the rewetting type quench, the so-called contact temperature was assumed to be the maximum liquid superheat and the rewetting temperature was obtained as follows:

$$T_R = T_M + K(T_M - T_L) \quad (2.8)$$

and

$$K = c(\lambda_L \cdot \rho_L \cdot c_{pL})^{0.5} / (\lambda_W \cdot \rho_W \cdot c_{pW})^{0.5} \quad (2.9)$$

where  $c$  is a factor to take into account the collision rate of the water to the heating wall, e.g.  $c$  is unity when the void fraction is 1.0 and  $c$  is zero when the void fraction is nearly 0.

In this analysis, it was assumed that  $c$  is unity and the cladding material is stainless steel, i.e. the following physical properties were used: For stainless steel

$$\lambda_W = 17.6 \quad (\text{Kcal/m} \cdot \text{h} \cdot ^\circ\text{C})$$

$$\rho_W \cdot g = 7860. \quad (\text{kg/m}^3)$$

$$c_{pW} = 0.118 \quad (\text{Kcal/kg} \cdot ^\circ\text{C})$$

and for water

$$\lambda_L = 0.586 \quad (\text{Kcal/m} \cdot \text{h} \cdot ^\circ\text{C})$$

$$\rho_L \cdot g = 1000. \quad (\text{kg/m}^3)$$

$$c_{pL} = 1.0 \quad (\text{kcal/kg} \cdot ^\circ\text{C})$$

Based on the above discussion, the quench model can be summarized as follows:

1.) For the dryout type quench

$$U_q = \frac{2361.2}{T_W - (321.05 + 0.237 \cdot 10^{-4} \cdot p)} \quad (\text{m/h}) \quad (2.10)$$

2.) For the liquid column type quench

$$U_q = \frac{2361.2(1+0.2778 \cdot 10^{-4} \cdot \Delta T_{\text{sub}}^3)}{T_w - (321.05 + 0.237 \cdot 10^{-4} \cdot p)} \quad (\text{m/h}) \quad (2.11)$$

3.) For the rewetting type quench

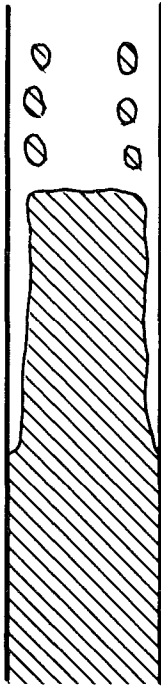
When the wall temperature falls down to the rewetting temperature  $T_R$ , the wall can be wetted by water and

$$T_R = 370.0 \quad (^\circ\text{C}) \quad (2.12)$$

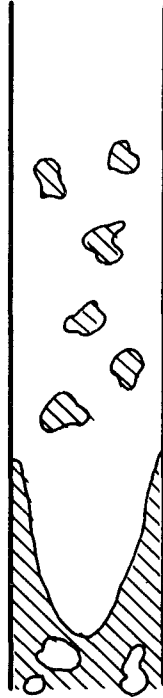
The heat flux was assumed to be equal to the maximum heat flux ( $\phi_{\text{MAX}}$ ).

The heat transfer characteristics were assumed to be the curve shown in Fig. 2-7, i.e. when the wall temperature falls down below the maximum liquid superheat, the heat flux increases up to maximum heat flux ( $\phi_{\text{MAX}}$ ) and in a short time the wall temperature falls down to the wall temperature corresponding to nucleate boiling. Then the wall temperature falls down along the line of nucleate boiling. That means that the wall temperature falls down automatically if the wall temperature can fall down to the maximum liquid superheat.

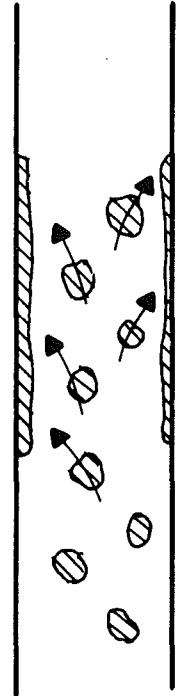
In the case of the dryout or liquid column type quench, the wall temperature falls down due to the axial heat conduction and in the case of the rewetting type quench, the wall temperature falls down due to redistribution of temperature profile between the wall and the coolant.



1) Liquid Column Type



2) Dryout Type



3) Rewetting Type

Fig.2-6

Three Types of the Quench Mode  
(Taken from Reference (5))

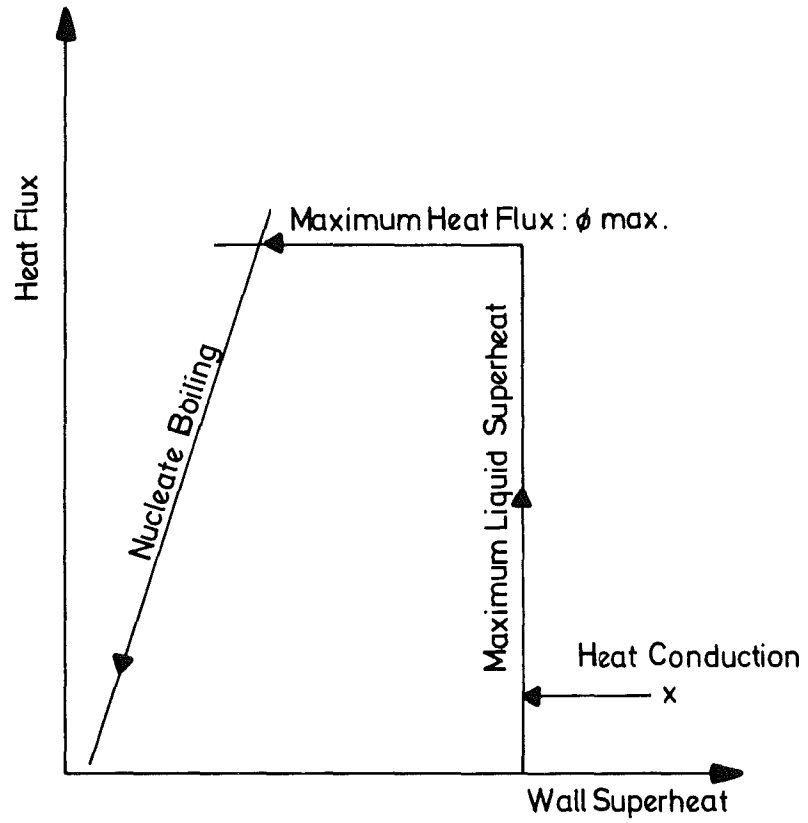


Fig. 2-7 Schematic Diagram of Heat Flux versus Wall Superheat  
( Taken from Reference (5) )

### 2.3 Thermo-hydrodynamics in the quenched region

In comparison with an ordinary condition, the flow velocity is relatively low under the reflood condition but the thermo-hydrodynamics were assumed to be described by ordinary thermo-hydrodynamic correlations.

It was assumed that:

1) For a heat transfer of single-liquid-phase forced convection, the Colburn's correlation is applicable to turbulent flow, i.e.

$$Nu = 0.023 \cdot Re^{0.8} \cdot Pr^{1/3} \quad (2.13)$$

and the lowest limit of the Reynolds number is extended to 2400.0 .

In the laminar flow region which is defined that Reynolds number is less than 2400.0, the following correlations are used<sup>(13)</sup>.

$$Nu = 1.077 \left( Re \cdot Pr \cdot \frac{D_e}{Z} \right)^{1/3} \quad (2.14)$$

$$Nu_{Min} = 3.65 \quad (2.15)$$

The upper correlation is called the solution by L  v  que. These correlations are well fitted with the Hansen's correlation<sup>(14)</sup>.

2) For a boiling heat transfer, the Jens and Lottes' correlation is applicable even in an annular flow region where it is sometimes enough to transfer heat by evaporation at the interface without forming many bubbles at the heated surface.

Where the Jens and Lottes' correlation is,

$$\phi_B = 2.197 (T_w - T_{sat})^4 \exp(1.54 \cdot 10^{-6} p) \quad (2.16)$$

Based on the assumption of the quench model, the maximum heat flux is taken as

$$\phi_{BMAX} = 3.43 \cdot 10^6 \cdot (1 + 0.2778 \cdot 10^{-4} \cdot (T_{sat} - T_L)^3) \quad (2.17)$$

3) For a frictional pressure loss of single-liquid-phase forced convection, the following well-known correlations are applicable to turbulent flow (Reynolds number is more than 2400.0)

$$F = 0.3166 \cdot \text{Re}^{-0.25} \quad (2.18)$$

to laminar flow (Reynolds number is less than 2400.0)

$$F = 64/\text{Re} \quad (2.19)$$

where F is the friction coefficient defined as follows:

$$F \equiv \gamma \frac{d\tau}{dZ} / \left( \frac{1}{2} \cdot \frac{\rho_L}{D_e} \cdot U_L^2 \right) \quad (2.20)$$

4) For a frictional pressure loss of subcooled boiling region, the above correlation is also applicable.

5) For a frictional pressure loss of bulk boiling two-phase flow, the Lockhart-Martinelli's<sup>(15)</sup> correlation with  $X_{tt}$  parameter is applicable, i.e.

$$\phi_L^2 = 1.0 + 20.0/X_{tt} + 1.0/X_{tt}^2 \quad (2.21)$$

where  $\phi_L^2$  is defined as

$$\phi_L^2 = \gamma \frac{d\tau}{dZ} / \left\{ \left( \frac{0.1875}{\text{Re}^{0.2}} \right) \frac{G^2 \cdot (1-X)^{1.8}}{2 \cdot \rho_L \cdot D_e} \right\} \quad (2.22)$$

6) For an equation of state of single-liquid-phase flow and subcooled boiling region, void fraction is taken as zero, i.e.

$$\alpha = 0 \quad (2.23)$$

7) For an equation of state of bulk boiling two-phase flow, the Lockhart-Martinelli's correlation with  $X_{tt}$  parameter is applicable, i.e.

$$\alpha = 1.0 - 1.0 / (1.0 + 21.0/X_{tt} + 1.0/X_{tt}^2)^{\frac{1}{2}} \quad (2.24)$$

## 2.4 Thermo-hydrodynamics in the unwetting two-phase flow region

### 1) Subcooled film boiling region

Measuring the vapor film thickness of pool film boiling, some workers thought that the comparatively high intensity of heat transfer cannot be interpreted on the basis of molecular heat conduction through the vapor layer. However, it is a consequence of the convection heat transfer inside the vapor film.

A number of papers have established that film boiling heat transfer from sufficiently long (height is more than 15.0 millimeter) vertical surface is insensitive to the linear dimension of the heated surface.

As the length is close to the so-called critical wave length which is derived from Taylor instability analysis and written as<sup>(16)</sup>

$$L_{crit} = 2\pi \left( \frac{\sigma}{g(\rho_L - \rho_g)} \right)^{1/2} \quad (2.25)$$

For a saturated film boiling heat transfer, the Bromley's correlation<sup>(17)</sup> is assumed to be applicable, i.e.

$$h_{sat} = 0.62 \cdot \left[ \frac{\lambda_g \cdot \rho_g \cdot (\rho_L - \rho_g) H_{fg} \cdot g}{L \cdot \mu_g \cdot (T_w - T_{sat})} \right]^{1/4} \quad (2.26)$$

where the physical properties of gas are defined for the mean temperature,

$$T_M = (T_w + T_{sat})/2 \quad (2.27)$$

and a linear dimension  $L$  is assumed to be equal to the critical wave length,

$$L = L_{crit} \quad (2.28)$$

The reason why the Bromley's correlation was adopted is as follows:

Sudo and the author developed the film boiling correlation using the experimental data obtained under the simulated reflood conditions. It was assumed that a linear dimension can be presented as a distance from the quench front and the coefficient of the Bromley's (Ellion's) correlation was determined as 0.94 instead of 0.62. The correlation agrees with the experimental data in the range of 5 to 10 centimeter distance from the quench front. If the linear dimension is assumed to be a critical wave length, the coefficient is in the range of 0.63 to 0.60. And so the Bromley's correlation with a coefficient of 0.62 was considered to be reasonable.

For a subcooled film boiling, the parameter of liquid subcooling is considered to be most sensitive and Kalinin <sup>(18)</sup> developed the correlation of a multiplication factor of the saturated film boiling with his data of liquid- nitrogen experiment. But for the water, the Kalinin's correlation was found to be not reliable.

Sudo and the author <sup>(6)</sup> developed the multiplication factor of the saturation film boiling for subcooled film boiling with their data and PWR-FLECHT data <sup>(11)</sup>.

The multiplication factor is written as

$$F = 1.0 + 0.025 \cdot (T_{\text{sat}} - T_L) \quad (2.29)$$

where F is a multiplication factor defined as

$$F \equiv h_{\text{sub}} / h_{\text{sat}} \quad (2.30)$$

The correlation predicts the heat transfer coefficient with the accuracy of ± 20 % error.

For a radiation heat transfer, assuming the emissivity factor is unity the following correlation was assumed to be added to the film boiling heat transfer.

$$h_R = \epsilon (T_W^4 - T_{\text{sat}}^4) / (T_W - T_{\text{sat}}) \quad (2.31)$$



where  $\epsilon$  is the Stephan-Boltzmann constant and  $\epsilon = 4.88 \cdot 10^{-8}$  (kcal/m<sup>2</sup>K<sup>4</sup>). The frictional pressure loss is assumed to be negligible, because the liquid phase does not contact the heated wall and the vapor film layer was considered as a lubricant.

## 2) Transition flow region

This region is difficult to describe with simple correlations. In the present stage, we have little information on it and have to adopt the simple correlation i.e. saturated film boiling correlation mentioned in 2.4 1) for heat transfer and a homogeneous two-phase flow model with slip between gas and liquid phase by use of the Lockhart-Martinelli correlation mentioned in 2.3 5) and 7) for hydrodynamics.

For a radiative heat transfer, the following correlation was assumed to be added to the saturated film boiling.

$$h_R = (1-\alpha)\epsilon \cdot (T_w^4 - T_{sat}^4) / (T_w - T_{sat}) \quad (2.32)$$

In this equation the emissivity factor is considered to be unity.

## 3) Dispersed flow region

In regard to the dispersed flow (mist flow), many workers studied it theoretically by use of so called "two-step model".

The two-step model takes into account (1) the heat transfer from the heated wall to the vapor flow and (2) the heat transfer from the vapor flow to the water droplets dispersed in the flow.

For the application of the two-step model, the determination of the droplet size and the slip velocity are important.

Many workers (e.g. Bennett, Forslund, and Groeneveld<sup>(9)</sup>) used the force balance between the drag force and the gravity force of

droplets, the Ingebo's<sup>(19)</sup> correlation for the drag coefficient of the droplets and the critical Weber number to solve the two-step model.

In this analysis, the same model was adopted, i.e.

- (1) The two-step model
- (2) The Ingebo's correlation written as follows

$$C_D = 27 \cdot Re_d^{-0.84} \quad (2.33)$$

- (3) The minimum drag coefficient

$$C_{DMIN} = 0.4 \quad (2.34)$$

- (4) The critical Weber number was assumed as 6.5 or 1.0

$$We \leq We_c = 6.5 \text{ or } 1.0 \quad (2.35)$$

where the Weber number is defined as

$$We \equiv \frac{\rho \cdot g \cdot \Delta U^2 \cdot D_d}{\sigma} \quad (2.36)$$

According to the Groeneveld's review<sup>(9)</sup>, the critical Weber number was measured by some workers as shown in Table 2-1. Groeneveld's recommended Isshiki's value, i.e.  $We_c = 6.5$

Table 2-1. Critical Weber Number  
(taken from reference (9)).

The Authors	We <sub>c</sub>	Note
Isshiki	6.5	For an accelerating air stream
Forslund	7.5	For dispersed nitrogen film boiling
Hinze	13	For a sudden acceleration
	22	For a gradual acceleration

(5) The force balance between the vapor flow and droplets.

$$C_D \cdot \frac{1}{2} \cdot \rho \cdot g \cdot \Delta U^2 \cdot \frac{\pi \cdot D_d^2}{4} = \frac{4}{3} \cdot \pi \cdot \left(\frac{D_d}{2}\right)^3 \cdot \rho_L \cdot g \quad (2.37)$$

(6)<sup>\*\*\*</sup> The heat transfer from the heated wall to the vapor flow is described by the same correlation as for the single-liquid phase with the physical properties of the vapor, i.e. equations (2.13), (2.14) and (2.15) are applicable.

(7)<sup>\*\*\*\*</sup> The frictional pressure loss between the heated wall to the vapor flow is described by the same correlation as for the single-liquid phase, i.e. equations (2.18), (2.19) and (2.20).

(8)<sup>\*</sup> The heat transfer from the vapor flow to the droplets can be described by the correlation for the convection heat transfer from the spherical bodies, i.e. for laminar flow ( $Re_d$  is less than 1800.0)

$$NU_{VD} = 2 + 0.55 \cdot Re_d^{0.5} \cdot Pr^{1/3} \quad (2.38)$$

for turbulent flow ( $Re_d$  is more than 1800.0)

$$NU_{VD} = 2 + 0.34 \cdot Re_d^{0.566} \cdot Pr^{1/3} \quad (2.39)$$

(9)<sup>\*\*</sup> The frictional pressure loss between the vapor flow and the droplets can be described by the left hand side of the equation (2.37) with the Ingebo's drag coefficient and the minimum drag coefficient, (2.33) and (2.34).

(10) The number flux of the droplets (defined as the number of droplets per unit area and unit time) can be written as follows with the mass balance of the liquid phase.

$$n = (1-\alpha)U_L / \left\{ \frac{4}{3} \cdot \pi \cdot \left(\frac{D_d}{2}\right)^3 \right\} \quad (2.40)$$

(11) ~~\*\*\*\*~~ The radiation heat transfer from the heated wall to the droplets can be added to the convective heat transfer and the radiation heat transfer is represented as by

$$h_{RWD} = F_s \cdot \epsilon \cdot (T_w^4 - T_{sat}^4) / (T_w - T_{sat}) \quad (2.41)$$

In the equation the emissivity factor is considered to be unity where  $F_s$  is a shape factor and defined as

$$F_s = \frac{s \cdot n}{U_L} \cdot \pi \cdot D_d^2 / C_\ell$$

$$F_{s_{Max}} = 1.0$$

(12) The effect of motion in the droplet was assumed to be negligible.

\* The equations (2.38) and (2.39) indicate the heat transfer for one droplet and the heat transfer rate from vapor to droplet based on the unit flow area. It is

$$(\gamma\phi)_{VD} = \frac{n}{C_\ell \cdot U_L} \cdot \frac{\lambda_g \cdot \pi \cdot D_d^2}{D_d} \cdot Nu_{VD} \cdot (T_g - T_{sat}) \quad (2.44)$$

Where  $\gamma$  is a ratio of the surface area to the area of the flow channel wall and the surface area means the total droplet surface area in this case.

\*\* The left hand side of the equation (2.37) indicates the frictional pressure loss for one droplet and the frictional force from vapor to droplets based on the unit flow area. It is

$$(\gamma \cdot \frac{d\tau}{dz})_{VD} = \frac{n}{U_L} \cdot C_D \cdot \frac{1}{2} \cdot \rho_g \cdot \Delta U^2 \cdot \pi \cdot \frac{D_d^2}{4} \quad (2.45)$$

\*\*\* Similarly, the heat transfer rate from wall to vapor based on the unit flow area is

$$(\gamma\phi)_{WV} = \frac{C_\ell}{s} \cdot \frac{\lambda_g}{D_e} \cdot Nu_{WV} \cdot (T_w - T_g) \quad (2.46)$$

\*\*\*\* Similarly, the frictional force from vapor to wall on the unit flow area is

$$\left(\gamma \frac{d\tau}{dz}\right)_{WV} = \frac{f \rho_g}{D_e} \cdot \frac{U_g^2}{2} = f' \frac{\rho_g U_g v_g}{2 D_e} \quad (2.47)$$

where  $f' \equiv f \cdot Re_D$

\*\*\*\*\* The radiative heat transfer from wall to droplets based on the unit flow area is

$$(\gamma \phi)_{WD} = \frac{C_{\ell}}{s} \cdot h_{RWD} \cdot (T_w - T_{sat}) \quad (2.48)$$

#### 4) Superheated steam flow region

The same correlations describing the single-liquid phase can be applied to superheated steam flow by using the physical properties of the steam, i.e.

For a heat transfer : equations (2.13), (2.14) and (2.15)

For a frictional pressure loss: equations (2.18), (2.19) and (2.20)

#### 5) The transition criteria from transition flow to dispersed flow

As mentioned in 2.4 3) , when the droplets are generated, the relation between the droplet size and the slip velocity can be presented by the combination of the equations (2.33), (2.34), (2.35), (2.36) and (2.37).

Arranging these equations, we can obtain the following correlation of the slip velocity as the transition criteria.

$$\Delta U_{crit} = \min (\Delta U_2 , \Delta U_3) \quad (2.49)$$

$$\text{where } \Delta U_2 = 0.53713 \cdot (\sigma \cdot \text{Wec})^{0.3801} \cdot \rho_g^{-0.5868} \cdot \tau^{-0.1736} \cdot (\rho_L \cdot g)^{0.2066}$$

$$\Delta U_3 = 1.3512 \cdot \left( \frac{\rho_L \cdot g \cdot \sigma \cdot \text{Wec}}{\rho_g^2} \right)^{0.25}$$

$\Delta U_{\text{crit}}$  is the critical slip velocity

and  $\min(a,b)$  indicates the minimum of the value a and b.

When the slip velocity exceeds the critical slip velocity, the droplets are assumed to be generated and the droplet size can be calculated as

$$D_d = \frac{\text{Wec} \cdot \sigma}{\rho_g \cdot \Delta U_{\text{crit}}^2} \quad (2.50)$$



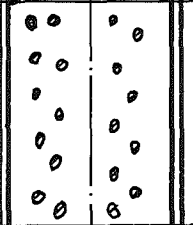
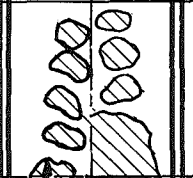
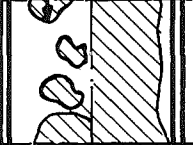
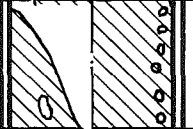

## 2.5 Summary of this chapter

As shown in Table 2.2, some flow regimes and thermohydrodynamic characteristics were assumed.

Where  $L_1$  to  $L_7$  are defined as follows:

- $L_1$  : bulk boiling point
- $L_2$  : quench point
- $L_3$  : start point of transition flow
- $L_4$  : start point of dispersed flow
- $L_5$  : start point of rewetted region
- $L_6$  : start point of bulk boiling in the rewetted region
- $L_7$  : start point of superheated steam flow, i.e. upper end of the water level

Table 2.2

Flow Pattern (saturated)(subcooled)	Flow Regime	Hydro-dynamic Model	Heat Transfer Model	Boundary Condition
	Super heated Steam Flow	Single Vapor Flow	Single Vapor Phase Forced Convection	over the top of liquid $\alpha > 0.9999999$
	Rewetted Regime	Wetting Two-Phase Flow	Nucleate Boiling and/or Single Liquid Phase	$T_w < T_q$ & $\alpha \leq 0.9999999$
	Dispersed Flow Regime	Unwetting Two-Phase Flow (Single Vapor Flow + Drag Force of Droplets)	Two-Step Model (Single Vapor Phase Forced Convection + Vapor to Droplets + Radiation to Droplets)	Slip Velocity > Free Fall Velocity of Droplets & $T_w \geq T_q$
	Transition Flow Regime	Unwetting Two-Phase Flow (Wetting Two-Phase Flow Correlation)	Saturated Film Boiling + Radiation	$T_w \geq T_q$ & $T_L = T_{sat}$
	Subcooled Film Boiling Regime	Unwetting Two-Phase Flow (Single Liquid Flow without Wall Friction)	Subcooled Film Boiling Correlation + Radiation	$T_w \geq T_q$ $T_L < T_{sat}$
	Bulk Boiling Regime	Wetting Two-Phase Flow	Nucleate Boiling	$T_w < T_q$ & $T_L = T_{sat}$
	Single-Liquid Phase Flow Regime	Single-Liquid Flow	Single Liquid Phase Forced Convection + Nucleate Boiling	$T_w < T_q$ & $T_L < T_{sat}$

( $L_6$  : bulk boiling  $P_t$  in rewetted regime,  $L_7$  : the upper end of the mater level)

### 3. MATHEMATICAL EXPRESSION OF PROBLEM

#### 3.1 Basic thermo-hydrodynamic equations for coolant in the quenched region and superheated steam flow region

Based on the assumption of homogeneous two-phase flow with slip between vapor and liquid phase, the Mac Farlane's method (15) can be used in these regions.

The Eulerian equations for conservation of mass, momentum, and energy for a two-phase fluid flowing upward in a vertical channel are:

Continuity

$$\frac{\partial}{\partial t} \{ \alpha \rho_g + (1-\alpha) \rho_L \} + \frac{\partial}{\partial Z} \{ \alpha \rho_g U_g + (1-\alpha) \rho_L U_L \} = 0 \quad (3.1)$$

Momentum

$$\begin{aligned} & \frac{\partial}{\partial t} \{ \alpha \rho_g U_g + (1-\alpha) \rho_L U_L \} + \frac{\partial}{\partial Z} \{ \alpha \rho_g U_g^2 + (1-\alpha) \rho_L U_L^2 \} \\ & + \frac{\partial p}{\partial Z} + g \{ \alpha \rho_g + (1-\alpha) \rho_L \} + \gamma \frac{\partial \tau}{\partial Z} = 0 \end{aligned} \quad (3.2)$$

Energy

$$\begin{aligned} & \frac{\partial}{\partial t} \{ \alpha \rho_g g \cdot H_g + (1-\alpha) \rho_L g H_L \} + \frac{\partial}{\partial Z} \{ \alpha \rho_g g U_g H_g + (1-\alpha) \rho_L g U_L H_L \} \\ & = \gamma \phi \left( = \frac{C_e}{s} \frac{\lambda}{D_e} Nu (T_w - T_L \text{ or } G) = \frac{C_e}{s} h (T_w - T_L \text{ or } G) \right) \end{aligned} \quad (3.3)$$

As an equation of state for two-phase flow, the void fraction is frequently correlated by the following expression with Lockhart-Martinelli two-phase flow parameter.

$$\alpha = F (X_{tt}) \quad (3.4)$$

where

$$X_{tt} = \left( \frac{1-x}{x} \right)^{0.9} \left( \frac{\rho_g}{\rho_L} \right)^{0.5} \left( \frac{\mu_L}{\mu_g} \right)^{0.1} \quad (3.5)$$



The two-phase frictional pressure gradient is frequently represented by an equation of the form

$$\gamma \cdot \frac{\partial \tau}{\partial Z} = F_2(X_{tt}) \quad (3.6)$$

Based on the assumption that thermodynamic equilibrium between liquid and vapor of the homogeneous two-phase flow is given and both temperatures are equal to the saturation temperature, i.e.

$$\rho_g = F_3(P) \quad (3.7)$$

$$\rho_L = F_4(P) \quad (3.8)$$

$$H_L = H_{sat} = F_5(P) \quad (3.9)$$

$$H_g = H_{sat} + H_{fg} = F_6(P) \quad (3.10)$$

If  $\phi$  is given under the suitable boundary and initial condition, these equations can be solved.

Considering eq. (3.8) (It means that liquid density is constant under constant system pressure), the following equation is obtained from eq. (3.2)

$$(\rho_g - \rho_L) \frac{\partial \alpha}{\partial t} + \frac{\partial G}{\partial Z} = 0 \quad (3.11)$$

Considering  $H_L$ ,  $H_g$ ,  $H_{fg}$ ,  $\rho_L$  and  $\rho_g$  are constant, from eq. (3.3)

$$\{\rho_g H_{fg} + (\rho_g - \rho_L) H_L\} \frac{\partial \alpha}{\partial t} + (X H_{fg} + H_L) \frac{\partial G}{\partial Z} + G H_{fg} \frac{\partial X}{\partial Z} = \gamma \phi \quad (3.12)$$

Since  $XG = G_g / \alpha = \rho_g U_g / \alpha$  and  $(1-X)G = G_L / (1-\alpha) = \rho_L U_L / (1-\alpha)$ , from eq. (3. )

$$\begin{aligned} & \frac{\partial G}{\partial t} + \frac{1}{\rho_L} \frac{\partial}{\partial Z} \left\{ G^2 \left( \frac{\beta X^2}{\alpha} + \frac{(1-X)^2}{1-\alpha} \right) \right\} \\ & + \frac{\partial p}{\partial Z} + g(\alpha/\beta + 1-\alpha) \cdot \rho_L + \gamma \frac{\partial \tau}{\partial Z} = 0 \end{aligned} \quad (3.13)$$

where  $\beta \equiv \frac{\rho_L}{\rho_g}$  (3.14)

Our problems to be solved are related to a problem of constant reflood rate and are relatively slow phenomena, and it can be assumed that  $\frac{\partial G}{\partial t} \approx 0$  and  $\frac{\partial \alpha}{\partial t} \approx 0$ .

Considering these condition, the following equations can be derived from eq.s (3.11), (3.12) and (3.13).

$$\frac{\partial G}{\partial Z} = 0 \quad (3.15)$$

$$\frac{\partial X}{\partial Z} = \frac{1}{G} \cdot \left( \frac{\gamma \phi}{H_{fg}} - ((1-X)\rho_g + X\rho_L) \frac{\partial \alpha}{\partial t} \right) \approx \frac{1}{G} \frac{\gamma \phi}{H_{fg}} \quad (3.16)$$

$$\frac{\partial p}{\partial Z} = - \frac{1}{\rho_L} \cdot \frac{\partial (V'G^2)}{\partial Z} - g \cdot \rho_L (\alpha/\beta + 1 - \alpha) - \gamma \frac{\partial \tau}{\partial Z} \quad (3.17)$$

where

$$V' = \frac{\beta X^2}{\alpha} + \frac{(1-X)^2}{1-\alpha} \quad (3.18)$$

The gas and liquid velocity can be easily derived from the definition of the quality.

$$U_g = XG / (\alpha \rho_{gsat}) \quad (3.19)$$

$$U_L = (1-X)G / ((1-\alpha)\rho_L) \quad (3.20)$$

For single phase flow, the following equations can be obtained similarly.

$$\frac{\partial G}{\partial Z} = 0 \quad (3.15')$$

$$\frac{\partial H_{L \text{ or } g}}{\partial t} + \frac{\partial (UH)_{L \text{ or } g}}{\partial Z} = \frac{\gamma \cdot \phi}{g \cdot \rho_{L \text{ or } g}} \quad (3.16')$$

$$\frac{\partial p}{\partial Z} = - \frac{1}{\rho_{L \text{ or } g}} \frac{\partial G^2}{\partial Z} - g \cdot \rho_{L \text{ or } g} - \gamma \frac{\partial \tau}{\partial Z} \quad (3.17')$$

### 3.2 Basic thermo-hydrodynamic equations for coolant in the un wetting two-phase flow

#### 1) Dispersed flow

Based on the assumption of perfectly separated two-phase flow, the Eulerian equations for conservation of mass, momentum and energy for a two-phase fluid flowing upward in a vertical channel are:

Continuity for vapor phase

$$\frac{\partial(\alpha \cdot \rho_g)}{\partial t} + \frac{\partial(\alpha \rho_g U_g)}{\partial Z} = \dot{Q} \quad (3.21)$$

Continuity for liquid phase

$$\frac{\partial\{(1-\alpha)\rho_L\}}{\partial t} + \frac{\partial\{(1-\alpha)\rho_L U_L\}}{\partial Z} = -\dot{Q} \quad (3.22)$$

Momentum for vapor phase

$$\begin{aligned} \frac{\partial(\alpha \rho_g U_g)}{\partial t} + \frac{\partial(\alpha \rho_g U_g^2)}{\partial Z} + \alpha \frac{\partial p}{\partial Z} + \alpha \rho_g g \\ + \left(\gamma \frac{\partial \tau}{\partial Z}\right)_{WV} + \left(\gamma \frac{\partial \tau}{\partial Z}\right)_{VD} = \dot{Q} U_L \end{aligned} \quad (3.23)$$

Momentum for liquid phase

$$\begin{aligned} \frac{\partial\{(1-\alpha)\rho_L U_L\}}{\partial t} + \frac{\partial\{(1-\alpha)\rho_L U_L^2\}}{\partial Z} + (1-\alpha) \frac{\partial p}{\partial Z} + (1-\alpha)\rho_L g \\ - \left(\gamma \frac{\partial \tau}{\partial Z}\right)_{VD} = -\dot{Q} U_L \end{aligned} \quad (3.24)$$

Energy for vapor phase

$$\frac{\partial(\alpha \rho_g g \cdot H_g)}{\partial t} + \frac{\partial(\alpha \rho_g g \cdot U_g \cdot H_g)}{\partial Z} = (\gamma \phi)_{WV} - (\gamma \phi)_{VD} + \dot{Q} g \cdot H_g \quad (3.25)$$

Energy for liquid phase

$$\frac{\partial\{(1-\alpha)\rho_L g H_L\}}{\partial t} + \frac{\partial\{(1-\alpha)\rho_L g U_L H_L\}}{\partial Z} = (\gamma\phi)_{VD} + (\gamma\phi)_{WD} - \dot{Q}gH_g \quad (3.26)$$

In order to express the characteristics of liquid droplets, the void fraction is given by the following correlation.

$$1 - \alpha = nV_d/U_L \quad (3.27)$$

As far as the liquid droplets are not fragmented, the number flux density of the liquid droplets must be kept constant.

Therefore

$$n = \text{constant} \quad (3.28)$$

The fragmentation of the liquid droplets has been discussed in 2.4.3).

Since the vapor density is a function of pressure and vapor enthalpy (or temperature), the vapor density can be expressed as

$$\rho_g = F_7(H_g, p) \quad (3.29)$$

Due to this assumption for the liquid enthalpy (or temperature) can be used the value at the saturation temperature.

$$H_L = H_{\text{sat}} \quad (3.30)$$

Expanding eq.(3.21)~ (3.26) with  $\frac{\partial\rho_g}{\partial p(z)} = 0$ ,  $\rho_L = \text{const}$ , the following equations can be obtained.

$$\frac{\partial\alpha}{\partial t} + \frac{\alpha}{\rho_g} \cdot \frac{\partial\rho_g}{\partial t} + U_g \cdot \frac{\partial\alpha}{\partial Z} + \frac{\alpha \cdot U_g}{\rho_g} \cdot \frac{\partial\rho_g}{\partial Z} + \frac{\alpha \cdot \partial U_g}{\partial Z} = \frac{\dot{Q}}{\rho_g} \quad (3.21')$$

$$- \frac{\partial\alpha}{\partial t} - U_L \cdot \frac{\partial\alpha}{\partial Z} + (1-\alpha) \cdot \frac{\partial U_L}{\partial Z} = - \frac{\dot{Q}}{\rho_L} \quad (3.22')$$

$$\begin{aligned} & \frac{\partial \alpha}{\partial t} + \frac{\alpha}{\rho_g} \cdot \frac{\partial \rho_g}{\partial t} + \frac{\alpha}{U_g} \cdot \frac{\partial U_g}{\partial t} + U_g \cdot \frac{\partial \alpha}{\partial Z} + \frac{\alpha U_g}{\rho_g} \cdot \frac{\partial \rho_g}{\partial Z} + 2\alpha \frac{\partial U_g}{\partial Z} + \frac{\alpha}{\rho_g U_g} \cdot \frac{\partial \rho}{\partial Z} \\ & + \frac{\alpha g}{U_g} + \frac{1}{\rho_g U_g} \cdot \{ (\gamma \frac{\partial \tau}{\partial Z})_{WV} + (\gamma \frac{\partial \tau}{\partial Z})_{VD} \} = \frac{\dot{Q} U_L}{\rho_g U_g} \end{aligned} \quad (3.23')$$

$$\begin{aligned} & - \frac{\partial \alpha}{\partial t} + \frac{1-\alpha}{U_L} \cdot \frac{\partial U_L}{\partial t} - U_L \cdot \frac{\partial \alpha}{\partial Z} + 2(1-\alpha) \frac{\partial U_L}{\partial Z} + \frac{1-\alpha}{\rho_L U_L} \cdot \frac{\partial p}{\partial Z} + \frac{(1-\alpha)g}{U_L} \\ & - \frac{1}{\rho_L U_L} \cdot (\gamma \frac{\partial \tau}{\partial Z})_{VD} = - \frac{\dot{Q}}{\rho_L} \end{aligned} \quad (3.24')$$

$$\begin{aligned} & \frac{\partial \alpha}{\partial t} + \frac{\alpha}{\rho_g} \cdot \frac{\partial \rho_g}{\partial t} + \frac{\alpha}{H_g} \cdot \frac{\partial H_g}{\partial t} + U_g \cdot \frac{\partial \alpha}{\partial Z} + \frac{\alpha U_g}{\rho_g} \cdot \frac{\partial \rho_g}{\partial Z} + \alpha \frac{\partial U_g}{\partial Z} + \frac{\alpha U_g}{H_g} \cdot \frac{\partial H_g}{\partial Z} \\ & = \frac{1}{\rho_g H_g} \cdot \{ \frac{(\gamma \phi)_{WV} - (\gamma \phi)_{VD}}{g} + \dot{Q} H_g \} \end{aligned} \quad (3.25')$$

$$- \frac{\partial \alpha}{\partial t} - U_L \frac{\partial \alpha}{\partial Z} + (1-\alpha) \frac{\partial U_L}{\partial Z} = \frac{1}{\rho_L H_L} \cdot \{ \frac{(\gamma \phi)_{VD} + (\gamma \phi)_{WD}}{g} - \dot{Q} H_g \} \quad (3.26')$$

Assuming the vapor as an ideal gas, we obtain the following equations:

$$H_g = H_{sat} + H_{fg} + C_{pg} \cdot (T_g - T_{sat}) \quad (3.31)$$

$$\rho_g = \rho_{gsat} \cdot (T_{sat} + 273) / (T_g + 273) \quad (3.32)$$

Subtracting eq. (3.22') from eq. (3.26') and arranging it with eq. (3.31),

$$\dot{Q} = \{ (\gamma \phi)_{VD} + (\gamma \phi)_{WD} \} / [ \{ H_{fg} + C_{pg} \cdot (T_g - T_{st}) \} g ] \quad (3.33)$$

Subtracting eq. (3.21') from eq. (3.25') and arranging it.

$$\frac{\partial H_g}{\partial t} + U_g \cdot \frac{\partial H_g}{\partial Z} = \frac{1}{\alpha \rho_g g} \cdot \{ (\gamma \phi)_{WV} - (\gamma \phi)_{VD} \} \quad (3.34)$$

As the fluid flow changes slowly, we can assume that the hydrodynamic behavior can be described as a quasi-steady state phenomenon.

Hence the time-differential terms can be eliminated from eq.(3.21') ~ (3.24').

Even if the term of  $(1/\rho_g)\partial p/\partial Z$  is assumed to be an order of the gravitational constant  $g$ , the term of  $(1/\rho_L)\partial p/\partial Z$  is an order of  $(\rho_g/\rho_L)g$ , i.e.  $1/250$  to  $1/1000$  of  $g$  at the pressure range of  $1$  to  $4(\text{kg/cm}^2)_a$ . Therefore the term of  $(1/\rho_L)\partial p/\partial Z$  in eq. (3.24') can be neglected.

Eliminating the time-differential terms and arranging other terms of eq. (3.21') ~ (3.24') with  $(1/\rho_L)\partial p/\partial Z = 0$ , the following equations can be obtained.

$$\frac{\partial(U_g\alpha)}{\partial Z} = \frac{\dot{Q}}{\rho_g} - \frac{\alpha U_g}{\rho_g} \cdot \frac{\partial \rho_g}{\partial Z} \equiv B1 \quad (3.35)$$

$$\frac{\partial\{U_L(1-\alpha)\}}{\partial Z} = \frac{\dot{Q}}{\rho_L} \equiv B2 \quad (3.36)$$

$$\frac{\partial p}{\partial Z} + \rho_g U_g \cdot \frac{\partial U_g}{\partial Z} = \frac{\dot{Q}}{\alpha} \cdot (U_L - U_g) - \rho_g g - \frac{1}{\alpha} \cdot \{(\gamma \frac{\partial \tau}{\partial Z})_{WV} + (\gamma \frac{\partial \tau}{\partial Z})_{VD}\} \equiv B3 \quad (3.37)$$

$$\frac{1}{2} \cdot \frac{\partial U_L^2}{\partial Z} = -g + \frac{1}{(1-\alpha)\rho_L} (\gamma \frac{\partial \tau}{\partial Z})_{VD} \equiv B4 \quad (3.38)$$

Further, assuming the change of kinetic energy within an unit of length is negligible in comparison to the change of potential energy within an unit of length, i.e.

$$\frac{1}{2} \cdot \frac{\partial U_L^2}{\partial Z} \ll g$$

Hence

$$B4 \equiv -g + \frac{1}{(1-\alpha)\rho_L} \cdot (\gamma \frac{\partial \tau}{\partial Z})_{VD} = 0 \quad (3.39)$$

Substituting eq. (2.40) and (2.45) into eq. (3.39),

$$B4 = -g + \frac{3}{4} \cdot C_p \cdot \frac{\rho_g}{\rho_L} \cdot \frac{(U_g - U_L)^2}{D_d} = 0 \quad (3.40)$$

The slip velocity  $\Delta U \equiv (U_g - U_L)$  is equal to the free fall velocity of a droplet and can be obtained from eq. (3.40) with the drag coefficient of the sphere,  $C_p$ , which is a function of  $\Delta U$  and

is given by eq. (2.33) and (2.34).

After  $\dot{Q}$  and  $H_g$  are solved from eq. (3.33) and (3.34),  $U_g$ ,  $U_L$ ,  $\partial p / \partial Z$  can be solved from eq. (3.35) ~ (3.37) with eq. (3.40), (2.33) and (2.34).

## 2) Transition flow

As we have only few information for transition flow, we assume that the basic hydrodynamic equation for coolant in the quenched region described in 3.1 can be applied for the transition flow.

## 3) Subcooled film boiling

The basic hydrodynamic equation in the single liquid flow region without pressure loss is applied for subcooled film boiling. The reason was described in 2.4 1)

### 3.3. Thermal equations in the fuel rod

To simplify the calculation, the one point model was adopted for the temperature calculation of the fuel rod. The axial heat conduction was neglected.

Hence the equation for calculating the temperature of the fuel rod can be written as,

$$C_{pF} \cdot \rho_F \cdot \frac{\partial T_W}{\partial t} = Q - \frac{C_\ell}{V_F} \cdot h_t \cdot (T_W - T_C) \quad (3.41)$$

where  $h_t$  is a total heat transfer coefficient, which is defined as

$$h_t = \{ (\gamma\phi)_{CONV} + (\gamma\phi)_R \} \cdot \frac{S}{C_\ell} / (T_W - T_C) \quad (3.42)$$

where  $T_C$  is a coolant temperature or a saturation temperature

$$\begin{aligned} \text{and if } T_w > T_{sat} + 0.0001 \text{ (}^\circ\text{C)} & \quad T_c \equiv T_{sat} \\ \text{if } T_w \leq T_{sat} + 0.0001 \text{ (}^\circ\text{C)} & \quad T_c \equiv T_L \end{aligned} \quad (3.43)$$

In the unwetted region, eq. (3.41) describes the increase or decrease of the temperature of the fuel rod.

But in the quenched region except just after quenching, the following equations is used to calculate how to release the stored energy in the fuel rod.

$$(\gamma\phi)_L = \frac{V_F}{S} \cdot (Q - C_{pF} \cdot \rho_F \frac{\partial T_w}{\partial t}) \quad (3.44)$$

where  $T_F$  is determined as a steady state calculation of temperature i.e.

$$T_w = \frac{Q V_F}{C_\ell h_t} + T_c \quad (3.45)$$

In the time just after quenching, the release of the stored energy from the fuel rod is calculated as follows,

$$(\gamma\phi)_\ell = \frac{V_F}{S} \{Q - C_{pF} \rho_F (T_{wo} - T_w) U_q\} \quad (3.46)$$

where  $U_q$  is the quench velocity and  $T_{wo}$  is the temperature of the fuel rod just before quenching. Such a temperature is called as the quench temperature and  $T_w$  is determined as

$$T_w = T_{sat} + 50.0 \text{ (}^\circ\text{C)} \quad (3.47)$$



#### 4. NUMERICAL CALCULATION

##### 4.1. Calculation method for dispersed flow

(1) Numerical calculation of energy equation

We have to solve eq. (3.34)

$$\frac{\partial H_g}{\partial t} + U_g \cdot \frac{\partial H_g}{\partial Z} = \frac{1}{\alpha \rho_g \cdot g} \cdot \{ (\gamma \phi)_{WV} - (\gamma \phi)_{VD} \} \quad (3.34)$$

to know the change of the gas enthalpy.

If we intend to use the usual finite difference method for solving the energy equation, we must encounter the trouble of instability of the calculation which is due to the strong sensitivity of the gas temperatures  $T_g$  in source term and we have further problems about selecting the time, space mesh to satisfy the criterion of Courant number  $C^* \leq 1$ , where  $C^*$  is  $U \Delta t / \Delta Z$ .

To avoid these problems, we will use the Lagrangian form of this equation, i.e.

$$\frac{DH_g}{Dt} = \frac{1}{\alpha \rho_g \cdot g} \cdot \{ (\gamma \phi)_{WV} - (\gamma \phi)_{VD} \} \quad (4.1)$$

The physical model of this equation is shown in Fig. 4.1, that is, the element of the fluid, which was positioned on the point of  $(Z - U_g \Delta t)$  at the time of  $(t - \Delta t)$ , flows to the point of  $Z$  and reaches this point at the time of  $t$ .

During the path between  $(Z - U_g \Delta t)$  and  $Z$ , heat is added to the element of fluid.

Assuming that the fluid velocity, the void fraction, the gas

density, heat transfer rates  $(\gamma\phi)_{WV}$  and  $(\gamma\phi)_{VD}$ , and the wall temperature vary slightly in one time step, the following approximate equation is obtained for the case that  $(\gamma\phi)_{WV}$  is greater than  $(\gamma\phi)_{VD}$ .

$$\frac{DH_g}{Dt} = A \cdot h_t \cdot (T_w - T_g) \quad (4.2)$$

where  $A = 1/(\alpha\rho_g gS)$   
 $h_t = h_{WV} - h_{VD} \cdot (T_g - T_{sat}) / (T_w - T_g)$

for the case that  $(\gamma\phi)_{WV}$  is less than  $(\gamma\phi)_{VD}$

$$\frac{DH_g}{Dt} = - A \cdot h_t \cdot (T_g - T_{sat}) \quad (4.3)$$

where  $A = 1/(\alpha\rho_g gS)$   
 $h_t = h_{VD} - h_{WV} (T_w - T_g) / (T_g - T_{sat})$

for the case that  $(\gamma\phi)_{WV}$  is equal to  $(\gamma\phi)_{VD}$

$$\frac{DH_g}{Dt} = 0 \quad (4.4)$$

Using eq. (3.31), the equations (4.2) to (4.4) can be transformed to the following equations

For  $(\gamma\phi)_{WV} > (\gamma\phi)_{VD}$

$$\frac{DT_g}{Dt} = \frac{A}{C_{pg}} \cdot h_t \cdot (T_w - T_g) \quad (4.2')$$

For  $(\gamma\phi)_{WV} < (\gamma\phi)_{VD}$

$$\frac{DT_g}{Dt} = \frac{A}{C_{pg}} \cdot h_t \cdot (T_g - T_{sat}) \quad (4.3')$$

For  $(\gamma\phi)_{WV} = (\gamma\phi)_{VD}$ , eq. (4.4) can be included in eq. (4.2) or (4.3), hence we include it in eq. (4.2').

For  $(\gamma\phi)_{WV} = (\gamma\phi)_{VD}$ , eq. (4.4) can be included in eq. (4.2) or (4.3), hence we include it in eq. (4.2').

The finite differential solutions of eq. (4.2') and (4.3') are derived as follows:

For  $(\gamma\phi)_{WV} \geq (\gamma\phi)_{VD}$

$$T_g(Z,t) = T_W + (T_g(Z-Ug\Delta t, t-\Delta t) - T_W) \exp\left(-\frac{Ahtt}{C_p g}\right) \quad (4.5)$$

For  $(\gamma\phi)_{WV} < (\gamma\phi)_{VD}$

$$T_g(Z,t) = T_{sat} + (T_g(Z-Ug\Delta t, t-\Delta t) - T_{sat}) \exp\left(\frac{Ahtt}{C_p g}\right) \quad (4.6)$$

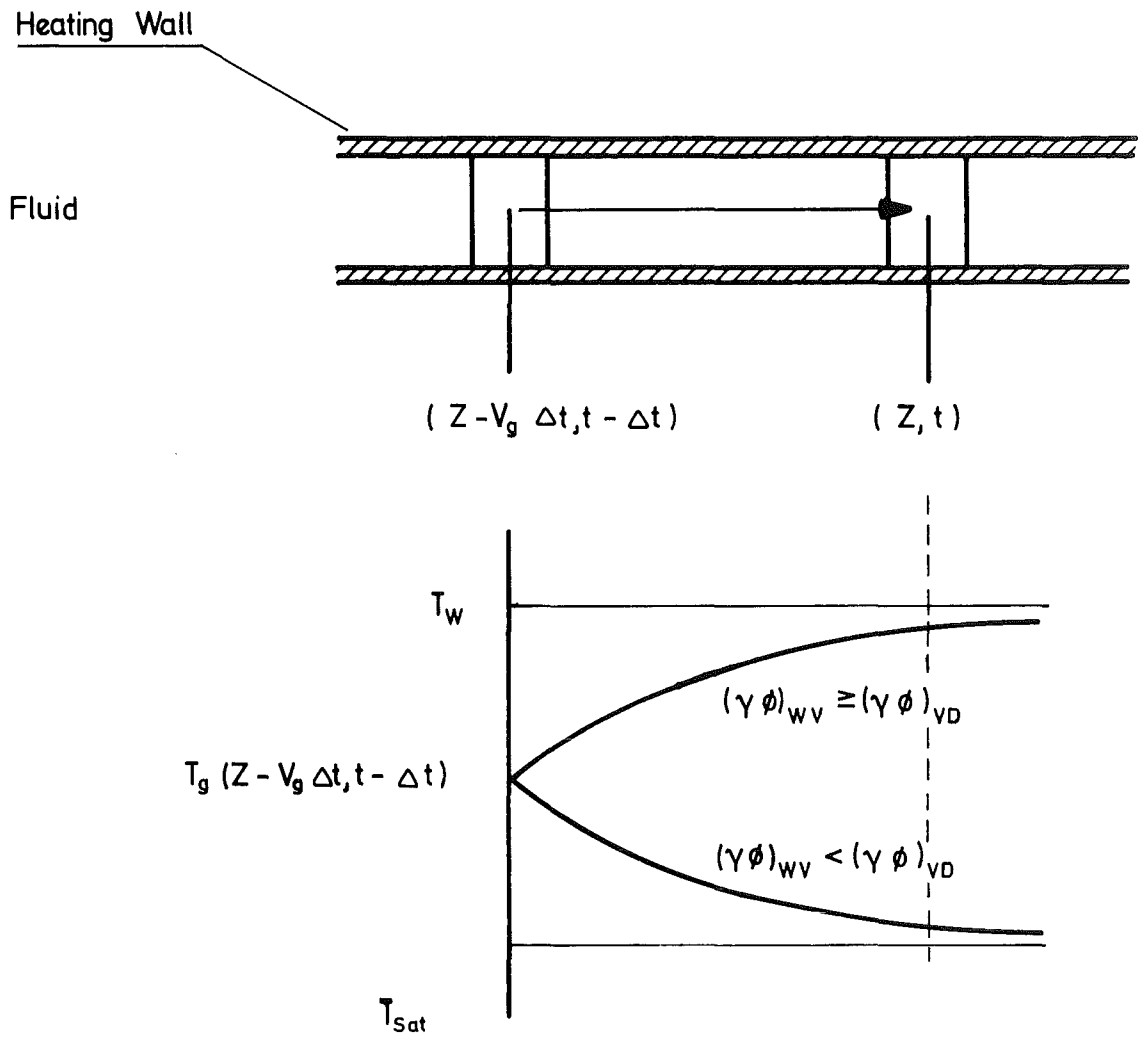


Fig. 4-1

Physical Model of the Lagrangian Energy Equation

(2) Numerical calculation of thermo-hydrodynamic equation

The finite differential forms of eq. (3.35) and (3.36) are written as

$$U_{gi+1} \cdot \alpha_{i+1} = U_{gi} \cdot \alpha_i + \Delta Z \cdot B1 \equiv C1 \quad (4.7)$$

$$U_{Li+1} \cdot (1-\alpha_{i+1}) = U_{Li} \cdot (1-\alpha_i) - \Delta Z \cdot B2 \equiv C2 \quad (4.8)$$

Using eq. (4.7) and (4.8) with  $\Delta U \equiv U_g - U_L$ , the void fraction  $\alpha$  can be expressed by the following equation.

$$\alpha_{i+1}^2 - \left(1 + \frac{C1 + C2}{\Delta U}\right) \alpha + \frac{C1}{\Delta U} = 0$$

Since  $\alpha_{i+1} < 1$ , and so

$$\alpha_{i+1} = \frac{1}{2} \left[ \left(1 + \frac{C1+C2}{\Delta U}\right) - \sqrt{1 + \frac{2(C2-C1)}{\Delta U} + \left(\frac{C1+C2}{\Delta U}\right)^2} \right] \quad (4.9)$$

From eq. (4.7)

$$U_{gi+1} = C1/\alpha_{i+1} \quad (4.10)$$

From the definition of the slip velocity

$$U_{Li+1} = U_{gi+1} - \Delta U \quad (4.11)$$

From eq. (3.37), we obtain the expression of the pressure

$$p_{i+1} = p_i + B3 \cdot \Delta Z (\rho_{gi} + \rho_{gi+1})/2 - (\rho_{gi}U_{gi} + \rho_{gi+1}U_{gi+1})/2 \cdot (U_{gi+1} - U_{gi}) \quad (4.12)$$

The slip velocity can be obtained from eq. (3.40), then we can obtain  $\alpha$ ,  $U_g$ ,  $U_L$ ,  $p$  using eq. (4.9) ~ (4.12).

#### 4.2 Calculation method for energy equation of liquid phase flow and superheated steam flow

Using eq. (3.31) and  $H_L = H_{sat} - C_{pL} \cdot (T_{sat} - T_L)$ , the following equation is described by eq. (3.16').

$$\frac{D H_{L \text{ or } g}}{Dt} = \frac{\gamma \phi}{(C_p \cdot \rho g)_{L \text{ or } g}} \quad (4.13)$$

Using a similar way as 4.1 (I), we obtain as

$$T_{L \text{ or } g}(Z, t) = T_w + T_{L \text{ or } g}(Z - U_{L \text{ or } g} \Delta t, t - \Delta t) - T_w \exp\left(-\frac{Ah_t t}{C_{pL \text{ or } g}}\right) \quad (4.14)$$

where  $A = 1/(\rho_{L \text{ or } g} g s)$   
 $h_t = h_{CONV}$

#### 4.3 General calculation method

Except above-mentioned equations, the finite difference method (the forward difference method), was adopted.

#### 4.4. Transition from the forced convection heat transfer to the boiling heat transfer

From eq. (2.16) and (2.17), we can obtain the wall temperature during boiling heat transfer  $T_{wBOIL}$ .

$$T_{wBOIL} = \left( \frac{\min(\phi_{BMAX}, \phi)}{2.197 \exp(1.54 \times 10^{-6} p)} \right)^{\frac{1}{4}} + T_{sat} \quad (4.15)$$

And if  $T_{wBOIL} < T_{wCONV}$ , the forced convection heat transfer is replaced by the following boiling heat transfer:

$$h_t \text{ BOIL} = \min(\phi_{B \text{ MAX}}, \phi) / (T_{w \text{ BOIL}} - T_{sat}) \quad (4.16)$$

#### 4.5 Structure of the computer program

As shown in Fig. 4.2, the calculation is carried out in the computer, i.e. (1) The input data are read. (2) Geometrical dimensions and physical properties (They depend on the system pressure) are calculated.

(3) The start of reflooding is calculated. (4) The boundaries (e.g. bulk boiling point, quench point, the upper end of subcool film boiling, transition flow and dispersed flow, and the lower end of rewetted region) are calculated. (5) The fuel temperature of the unwetted region is calculated. (6) The behavior of the thermo-hydrodynamics of the coolant and the fuel temperature of quenched region are calculated. (7) The results are printed or stored.

The sequence from (4) to (7) is repeated until the terminate condition is satisfied.

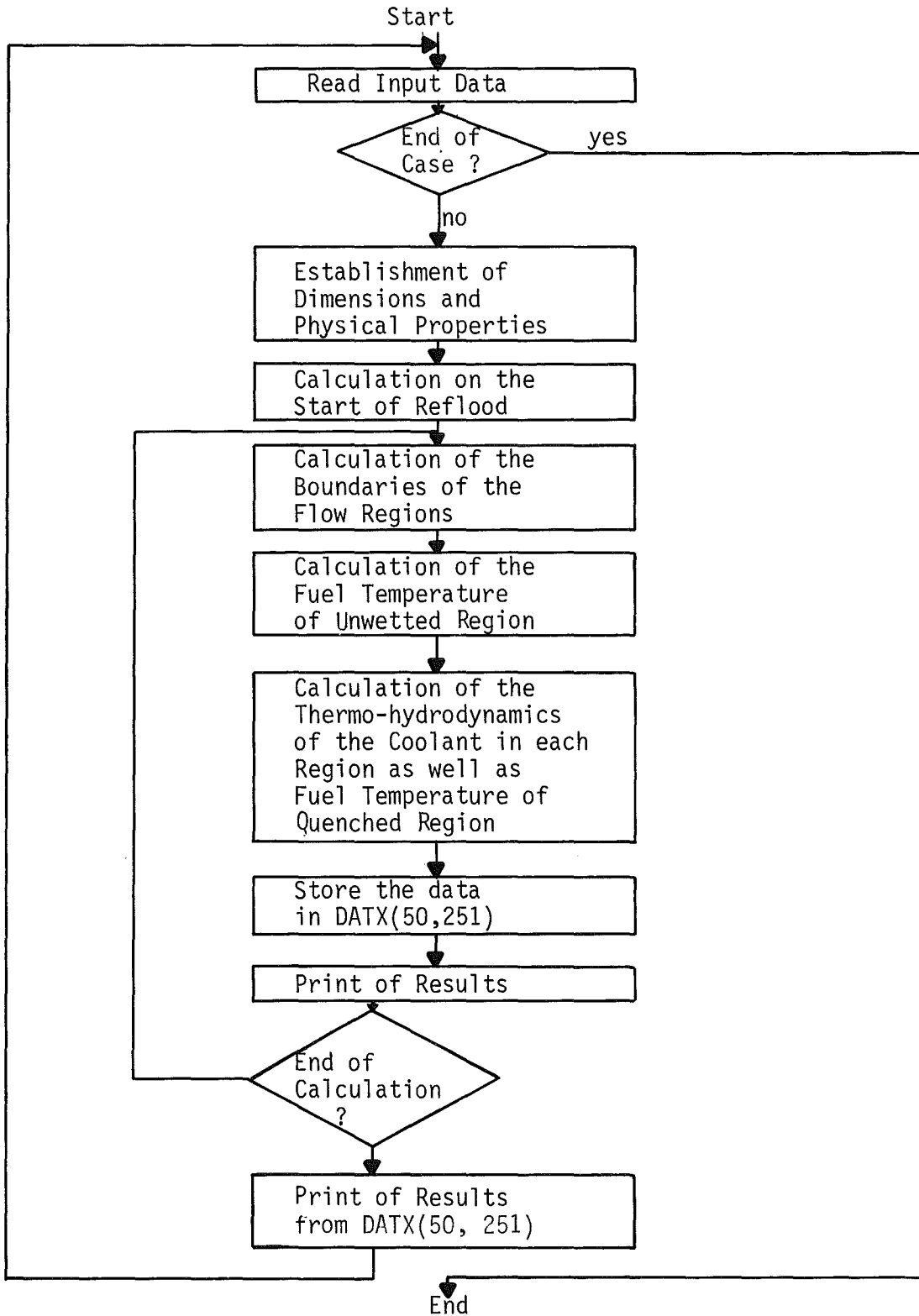


Fig. 4.2 Flow Diagram of the Calculation



#### 4.6 Power distribution and decay heat curve

The axial power distribution can be calculated from Subroutine SBPA (PX, J), where J is the axial node number and PX is the normalized power at the node J.

The power distribution is shown in Fig. 4.3 and is controlled by IAXMOD (It is one part of the input data).

The decay heat curve can be generated by the Function Program FQT(TM), where FQT is a normalized linear power and TM is a time in second.

Four types of decay curve have been implemented as follows.

- 1) The 1.2 times of ANS Standard (20) fission product decay heat.

$$\begin{array}{ll} TM < 9.9: & FQT = P\bar{O} \cdot 0.0603 \cdot (TM+0.1)^{-0.0639} \\ 9.9 \leq TM < 149.9: & FQT = P\bar{O} \cdot 0.0766 \cdot (TM+0.1)^{-0.181} \\ 149.9 \leq TM < 4 \cdot 10^6: & FQT = P\bar{O} \cdot 0.130 \cdot (TM+0.1)^{-0.283} \\ TM \geq 4 \cdot 10^6: & FQT = P\bar{O} \cdot 0.266 (TM+0.1)^{-0.335} \end{array}$$

- 2) B Type curve of PWR-FLECHT (10 x 10 Bundle)

$$FQT = 0.4200 \exp(-0.0283 \cdot TM) + 0.5800 - 3.920 \cdot 10^{-4} \cdot TM$$

- 3) A Type curve of PWR-FLECHT (7 x 7 Bundle)

$$FQT = 0.4518 \exp(-0.0283 \cdot TM) + 0.5482 - 4.922 \cdot 10^{-4} \cdot TM$$

- 4) The decay curve for JAERI'S experiment  $FQT = 1.0$

By fixing I in the Function Program FQT (TM), we can use the desired decay curve.

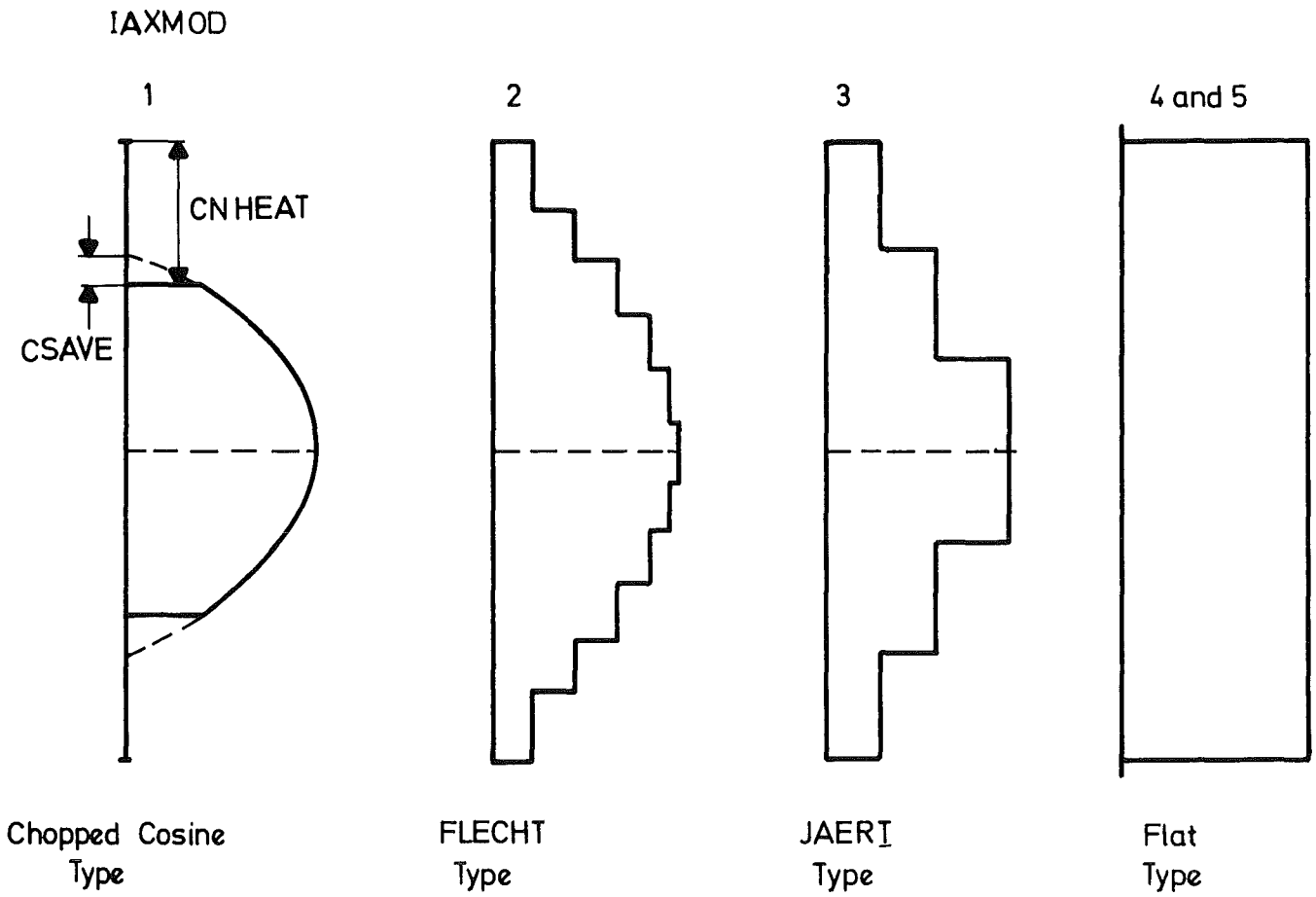


Fig. 4-3

Axial Power Distribution

#### 4.7 Control sequence of the calculation

The calculation is controlled by the sequence shown in Fig. 4.4, i.e.

(1) Before reflood, the fuel temperature increases and reaches a given temperature, TEMP2. Then the injection of water starts and begins to fill the lower plenum.

(2) When the lower plenum is filled with the water, reflood of core starts and after a given time, TIME3, the flow velocity is changed from ULIN2 to ULIN3. During reflood, the power is gradually decreased corresponding to a function like the decay heat curve.

(3) At a given time TIME4 after quenching of the middle point of fuel rod or at a given time TIME5 after reflooding, or at the time when the temperature of the middle point of the fuel rod exceeds a given temperature TEMP5, the calculation is turned to end.

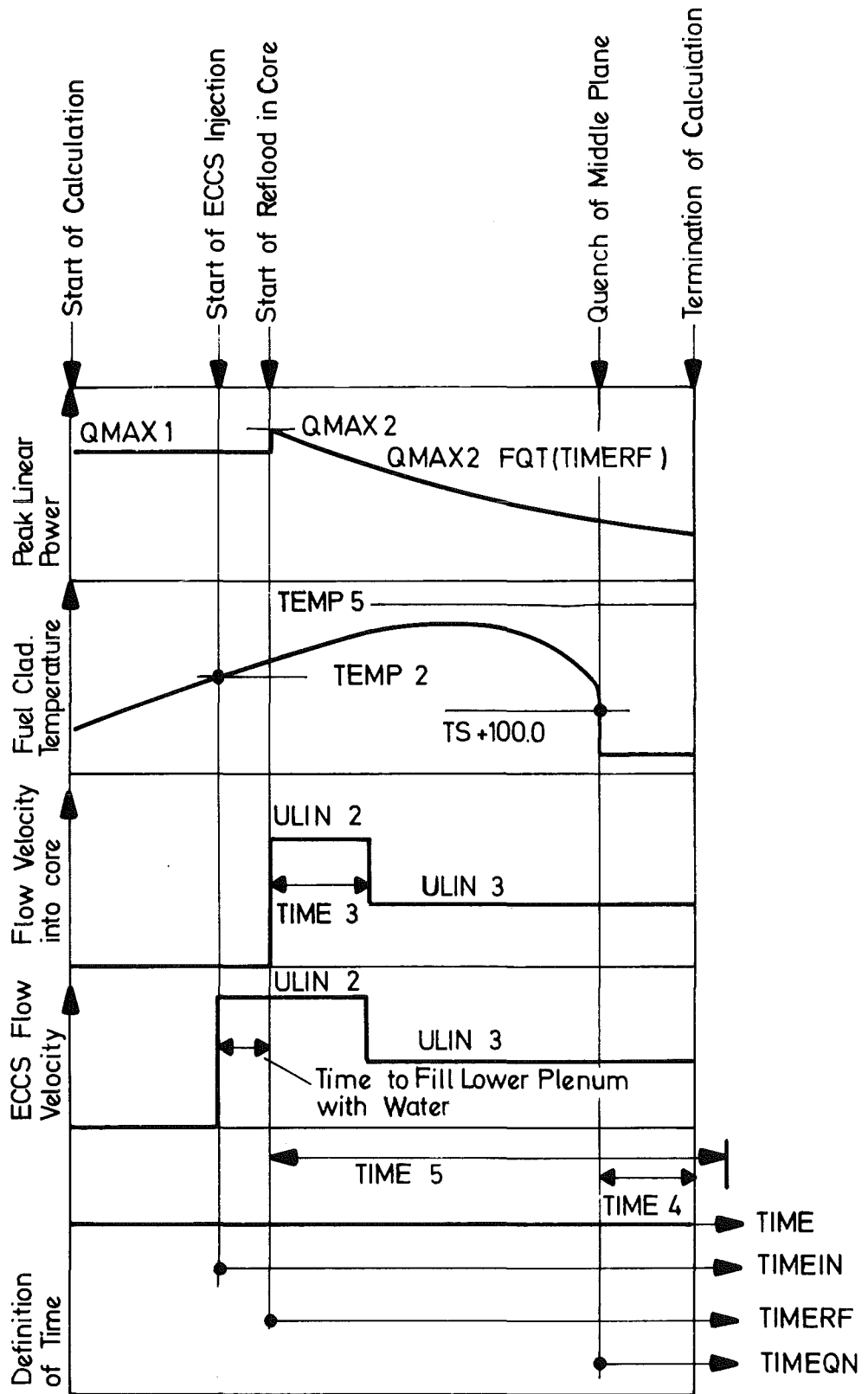


Fig. 4-4

Control Sequence of the Calculation

4.8 Logics for determining the boundaries of the regions

First, the quench fronts ( $L_2^*$ ,  $L_5^*$ ) and the water level ( $L_7^*$ ) are determined, i.e.

- (1)  $L_2$  can be calculated from the quench velocity (ULIB2).
- (2)  $L_5$  can be calculated from the quench velocity (ULIB5), which is zero under the condition that the clad temperature of the top of the fuel is higher than the rewetting temperature.
- (3)  $L_7$  can be calculated from the water velocity.  
Using the following logics, the quench point can be fixed.
- (4)  $L_2 \leq L_7$
- (5)  $L_5 \leq L_7$

The additional logics shown in Table 4.1 determine the  $L_1^*$ ,  $L_3^*$ ,  $L_4^*$ ,  $L_6^*$  and if the quality at  $L_7$  is larger than unity,  $L_7$  can be modified as the highest point where the quality  $X$  is less than unity.

\*  $L_1$  to  $L_7$  are defined in Table 2.2.

Table 4.1

Logics for determination of the boundaries

Position of Boundaries	$\alpha = 0$ $T_L < T_s$	$0 < \alpha < 0.9999999$ $T_L = T_s$	$\alpha = 1$ $X \geq 1.0$
$L_1$	SINGLF	$L_2$	$L_2$
$L_3$	SINGLF	$L_2$	$L_2$
$L_4$	$L_7$ /TRNSRM	$L_7$ /TRNSRM	$L_7$ /TRNSRM
$L_6$	SINGLF	$L_5$	$L_5$

SINGLF means that the position is determined in subroutine SINGLF.  $L_7$ /TRNSRM means that usually the position is equal to  $L_7$  but when the dispersed flow regime exists, the position is determined in subroutine TRNSRM (SINGLF: Single phase flow regime, TRNSRM: Transition flow regime).

4.9 Form of Input Cards

Table 4.2

(1/3)

Card Group	Card Number (Format)	Field	Variable	Unit	General Description	Remarks
Core Data	1  (2I12,3E12.5)	1	N	-	Number of rod cross section	
		2	IFBMOD	-		1 ~ 100 mm
		3	DIA	mm,m	Diameter of rod	0.001 ~ 0.1 m
		4	PITCH	mm,m	Pitch of rod array	1 ~ 100 mm 0.001 ~ 0.1 m
		5	CLENG	mm,m	Length of rod	If PITCH = 0,0 , flow channel is cylindrical tube and the equivalent diameter = DIA  10 ~ 5000 mm 0.01 ~ 5 m
Control Data	2  (5E12.5)	1	WEC	-		
		2	0.0	-		
		3	DTS	sec	Time step	
		4	TPRINT	sec	Time interval of printing data	
		5	VOL	m <sup>3</sup> /n <sup>2</sup>	Lower plenum volume divided by flow channel area	

(Continued)

(2/3)

Card Group	Card Number (Format)	Field	Variable	Unit	General Description	Remarks
Fuel Properties	3 (I12,4E12.5)	1	0	—	Conductivity of fuel Density of fuel Specific heat of fuel	
		2	0.0	—		
		3	CKF	kcal/mhK		
		4	DF	kg/m <sup>3</sup>		
		5	CF	kcal/kgK		
Axial Power Distribution	4 (I,2E12.5)	1	IAXMOD	-	Axial power distribution mode	see Fig.4.3
		2	CNHEAT	m	Non-heated length at each end	If IAXMOD ≠ 1 CNHEAT = 0.0
		3	CSAVE	m	Core saving	CSAVE = 0.0
Sequence Control Data	5 (6E12.5)	1	0.0			see Fig. 4.4
		2	TEMP1	°C	Initial wall temperature	If TEMP1 = 0.0 TEMP1 = TS
		3	QMAX1	kW/m	Initial peak linear power	TW = TS
		4	0.0			IF TEMP1>0.0 TW = TEMP1
		5	PSYS1	(kg/cm <sup>2</sup> ) <sub>a</sub> psia	System pressure	TS:Saturation Temp.
		6	TLIN1	°C	Injected coolant temperature	TW: Clad Wall Temp.
					If TLIN1 < 0.0 TLIN1 =  TS - TLIN1  (TS:Saturation Temp.)	

(Continued)

(3/3)

Card Group	Card Number (Format)	Field	Variable	Unit	General Description	Remarks
Sequence Control Data	6 (4E12.5)	1 2 3 4	0.0 TEMP 2 QMAX 2 ULIN2	- °C kW/m cm/sec	ECCS start temperature Linear power at reflood start Injection velocity of coolant	See Fig. 4.4
(Continued)	7 (4E12.5)	1 2 3 4	TIME3 0.0 0.0 ULIN3	sec - - cm/sec	Injection velocity is ULIN2 for TIME3 sec after reflood start  2nd injection velocity after TIME 3	
	8 (E12.5)	1	TIME4	°C	Termination time of calculation after quench of midplane	
	9 (2E12.5)	1 2	TEMP5 TEMP5	sec °C	Maximum computing time Maximum fuel temperature for termination of calculation	



4.10 Stored output data

DATX (50,251) is the data array for the stored output data and (DATX (J, NPRINT), J = 1, 50) are defined as Table 4.3.

Table 4.3 Description of the Stored Output Data

J	Name of Variables	Unit
1	time after reflood	sec
2	peak linear heat rate	kW/m
3	injection flow velocity	cm/sec
4	system pressure	(kg/cm <sup>2</sup> ) <sub>a</sub>
5	clad surface temperature	°C
∫	at the 1/6 elevation of core	∫
∫	∫	∫
10	6/6	°C
11	total heat transfer coeff.	kcal/m <sup>2</sup> hK
∫	at the 1/6 elevation of core	∫
∫	∫	∫
16	6/6	kcal/m <sup>2</sup> hK
17	void fraction	-
∫	at the 1/6 elevation of core	∫
∫	∫	∫
22	6/6	-
23	gas phase temperature	°C
∫	at the 1/6 elevation of core	∫
∫	∫	∫
28	6/6	°C

Table 4.3 Description of the stored output data (continued)

J	Name of Variables	Unit
29	coolant subcooling at quench point	<sup>o</sup> C
30	quench velocity	cm/sec
31	entrainment carry-over ratio	
32	apparent water level	m
33	L1:bulk boiling pt.	m
34	L2:quench point	m
35	L3:start pt. of transition flow	m
36	L4: start pt. of dispersed flow	m
37	L5: start pt. of rewetted region	
38	L7: start pt. of super- heated steam flow	m
39	differential pressure head of core	m
40	fraction of radiation heat transfer to total heat transfer	m
41	0.0	m
42	L6: start pt. of bulk boiling in rewetted region	m

Table 4.3 Description of the stored output data  
(continued)

J	Name of Variables	Unit	
43	lower quench temperature	°C	
44	upper quench temperature	°C	
45	lower quench node	-	
46	upper quench node	-	

#### 4.11 Sample input data

The three runs were taken as sample input data from PWR-FLECHT data.

Table 4.4

Experimental Conditions of Sample Runs

Run No.	(unit)	3541	4225	5123
Initial Wall Temp.	°C	140.0	140.0	140.0
Maximum Wall Temp.	°C	870.0	870.0	870.0
Maximum Power Density	kW/m	4.068	4.068	4.068
Flooding Velocity	m/h	539.36	173.69	173.69
	cm/sec	14.98	4.83	4.83
Coolant Subcooling	°C	82.22	85.0	30.56
System Pressure	kg/cm <sup>2</sup>	4.084	4.149	3.858
Housing Temp.	°C	241.1	307.8	316.1

In table 4.5, the example of input cards is shown using the experimental condition of PWR-FLECHT Run #3541.

Table 4.5 The Example of Input Cards

column card number	1 ~ 12	13~24	25~36	37~48	49~60	61~72
1	N 90		DIA 10.7	PITCH 14.3	CLENG 3.6	
2	WEC 1.0		DTS 0.05	TPRINT 2.0	VOL 0.0	
3			CkF 10.8	DF 2000.0	CF 0.41318	
4	IAXMOD 2					
5		TEMP1 140.0	QMAX1 4.068		PSYS1 4.084	TLIN1 -82.22
6		TEMP2 870.0	QMAX2 4.068	ULIN2 14.98		
7	TIME3 500.0			ULIN3 14.98		
8	TIME4 50.0					
9	TIME5 500.0	TEMP5 1300.0				

Note 1. These data were taken from  
PWR-FLECHT Run #3541

Note 2. When the case of the calculation is the last one, the blank  
card should be added at the next of No. 9 card.

## 5. RESULTS AND DISCUSSION

### 5.1 Temperature histories

The calculated temperature histories (shown by the solid lines) were compared with the measured curves (shown by the dotted line) in Fig. 5.1 to 5.3 for three cases described in Table 4.4. In the first case, the clad temperatures were calculated with critical Weber number  $We_c = 6.5$  and  $1.0$ . The both calculated results, but specially for  $We_c = 1.0$ , almost agreed with the measured curve as shown in Fig. 5.1. This PWR-FLECHT run # 3541 is characterized by a high inlet velocity and high coolant subcooling.

In the second case, the clad temperature were calculated with critical Weber number  $We_c = 6.5$ ,  $1.0$  and  $1/6.5$  as shown in Fig. 5.2. The calculated result for  $We_c = 1.0$  seems to be better than the others but even the result for  $We_c = 1.0$  does not so agree with the measured curve. This PWR-FLECHT run # 4225 is characterized by a low inlet velocity and a high coolant subcooling.

In the third case, the calculated clad temperatures for  $We_c = 0.5$  and  $1.0$  are shown in Fig. 5.3. The result for  $We_c = 1.0$  also seems to be better and agrees nearly with the measured. This PWR-FLECHT run # 5123 is characterized by a low inlet velocity and a low coolant subcooling.

In Fig. 5.2 and 5.3, the transition flow regions are indicated and it is found that the calculated heat transfer coefficient for this region is higher than the measured in earlier stage, but lower in later stage.

The reason why they are somewhat different from measured curves is mainly that the heat transfer correlation of the transition flow region is not suitable. Hence a further investigation on

the transition flow region seems to be important to develop the reflood code.

## 5.2 Effects of critical Weber number

The effects of critical Weber number on the thermo-hydrodynamics were examined by calculating the temperature histories and the water droplet size by variation of the critical Weber number.

As shown in Fig. 5.2, the variation of the critical Weber number influences the temperature histories. But we should note that the critical Weber number determines the initiation time of the transition flow and does not affect so much the heat transfer in the dispersed flow region which exists before the transition flow initiates.

In Table 5.1, the calculated water droplet size is shown with variation of the critical Weber number for three cases.

The observed water droplet diameter by Schmidt <sup>(8)</sup> is about 1.0 to 0.5 millimeter. The calculated results for  $We_c = 1.0$  are in the observed range.

Table 5.1

Calculated Water Droplet Size  
- Average Diameter (mm)

Critical Weber Number $We_c$	3541	Run Number 4225	5123
6.5	2.5	2.4	2.4
1.0	0.91	0.90	0.94
$\frac{1}{6.5}$	* —	0.33	* —

\* not calculated



### 5.3 Check of quench model

The quench positions for the three FLECHT runs are plotted versus time in Fig. 5.4. Generally the agreements of the measured and of the calculated results are considerably good and the affection of the critical Weber number by the advance of the quench front is small. The calculation error for  $We_c = 1.0$  is within  $\pm 16$  seconds. But in earlier stage, before turnaround time the agreement could not be obtained and in that period, the agreement between measured and calculated temperature histories also could not be obtained. The improvement of this point is necessary.

On Table 5.2, the calculated quench temperatures are compared with the measured quench temperatures of PWR-FLECHT experiment which are respectively listed as two values which correspond to the data from two thermocouples. The determination of the quench temperatures is difficult, because the temperature is rapidly changed near the quench time. Therefore the determined quench temperature includes some uncertainties. Considering such a situation, the calculated results appear to be not bad.

On Fig. 5.5, the calculated and measured quench temperatures are plotted versus elevation for FLECHT Run # 3541. The calculated and measured one are different from each other by 100 to  $-25^{\circ}\text{C}$  but their tendency seems to be similar to each other.

The proposed quench model seems to express the quench phenomenon considerably well, but for rewetting type quench we could not check the quench model because only one case (Run # 3541) was including rewetting type quench which was slow in initiation and had much calculational instabilities.

As a calculation condition, heater rods were assumed to have 3.6 meter heated length and neglected the non-heated part because we had no information about upper non-heated part of the heater rods, and we could not specify the calculation condition of the part.

Maybe the initial surface temperature of the part is lower than the rewetting temperature. Therefore the rewetting type quench occurs in practical case if the water comes to the upper end of the heated part.

#### 5.4 Numerical Calculation

The calculation was relatively stable and the computing time is about the same as a real time for a IBM 370 computer.

That shows a new Lagrangian method is useful for solving energy equations of gas phase and dispersed flow region.

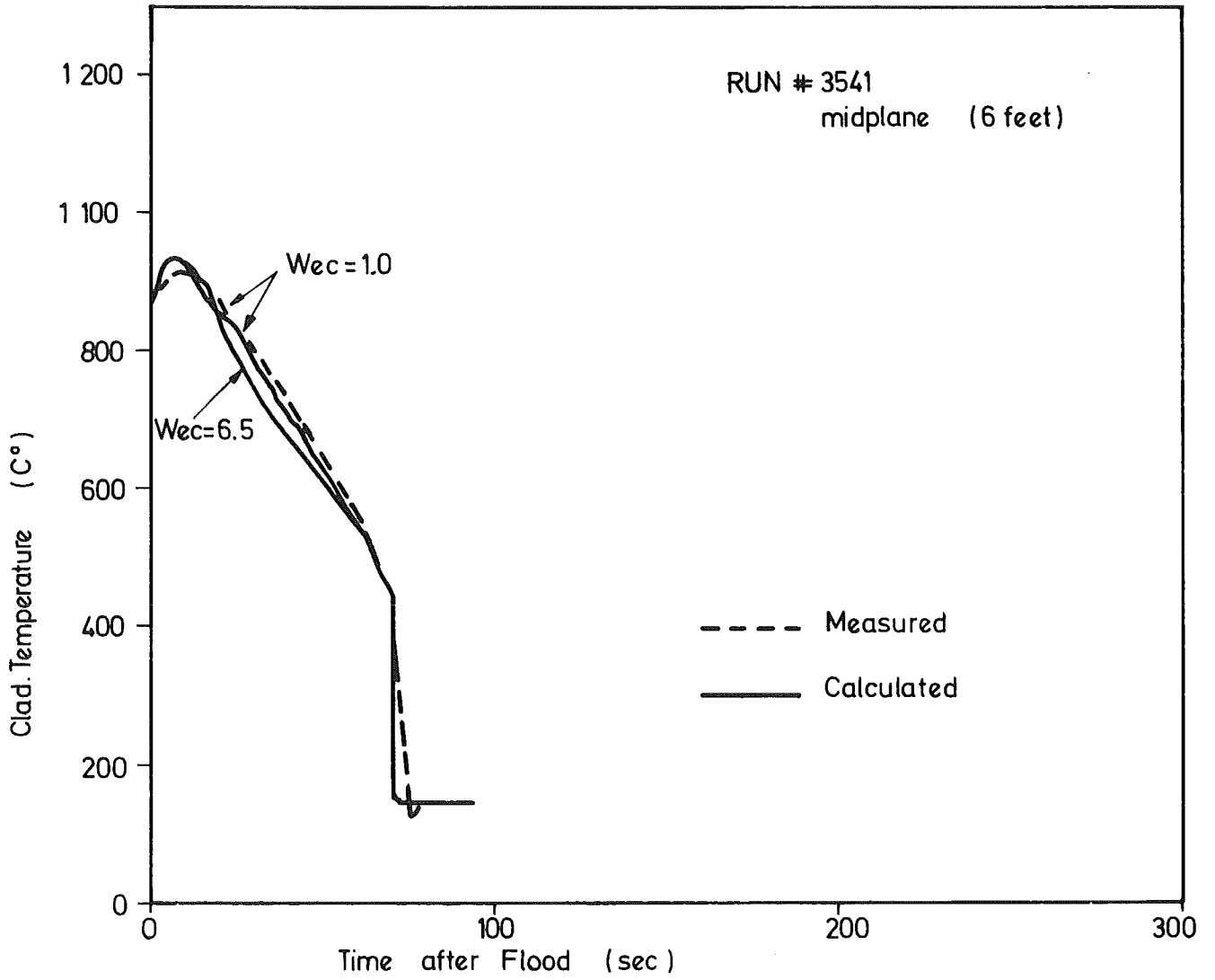


Fig. 5-1

Calculated Temperature History ( RUN # 3541 )

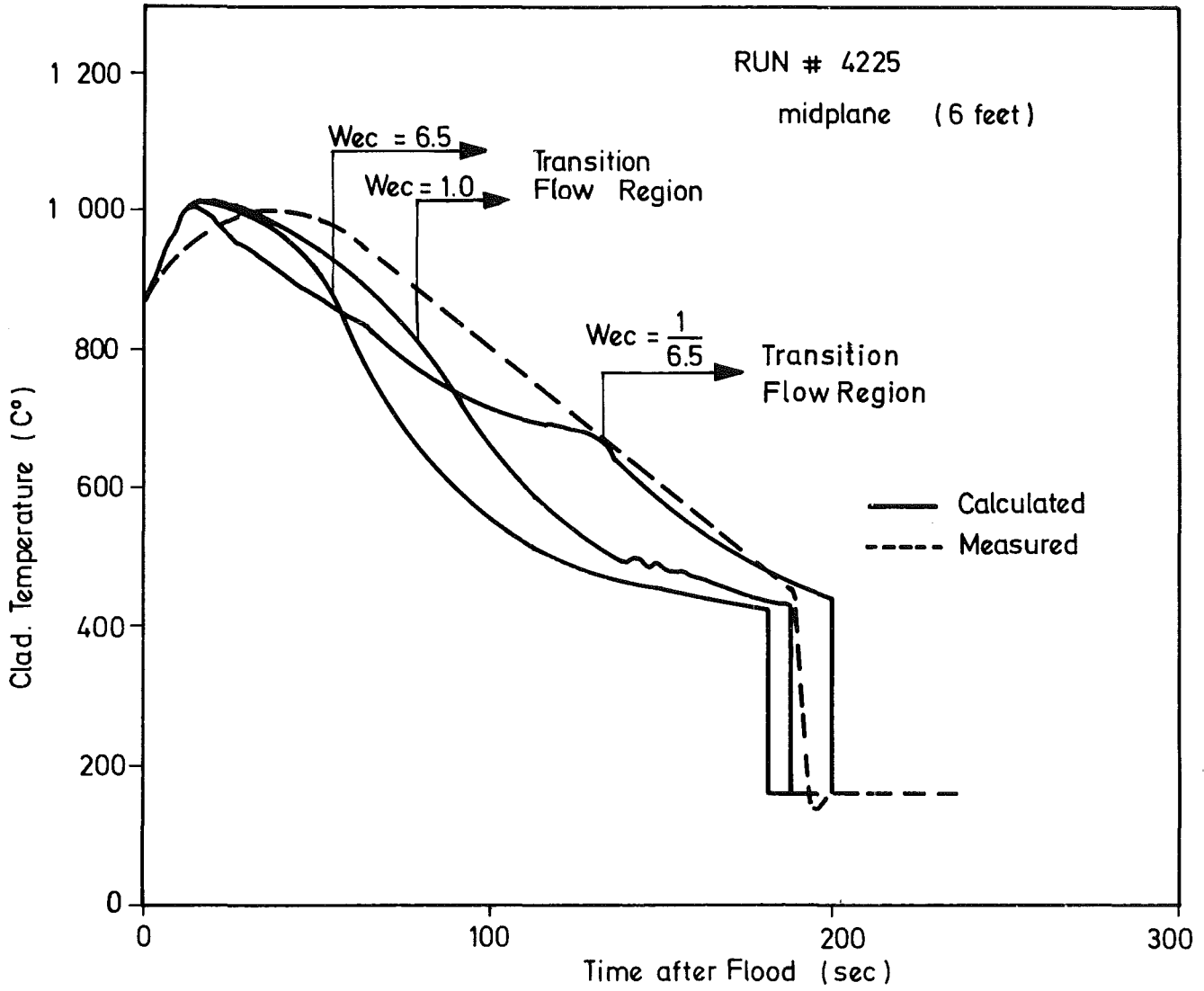


Fig. 5-2

Calculated Temperature History (RUN # 4225)

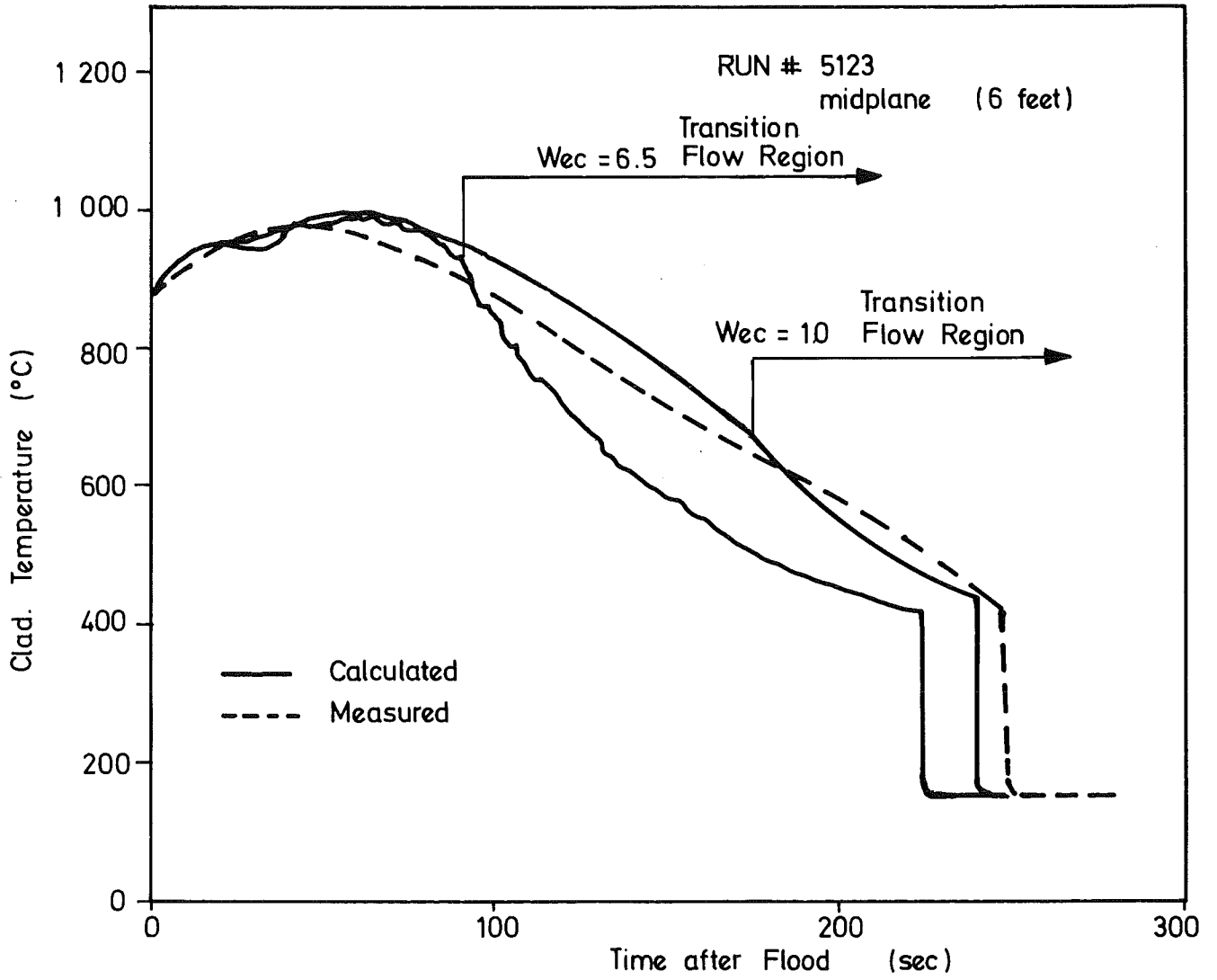


Fig. 5-3

Calculated Temperature History (RUN # 5123)

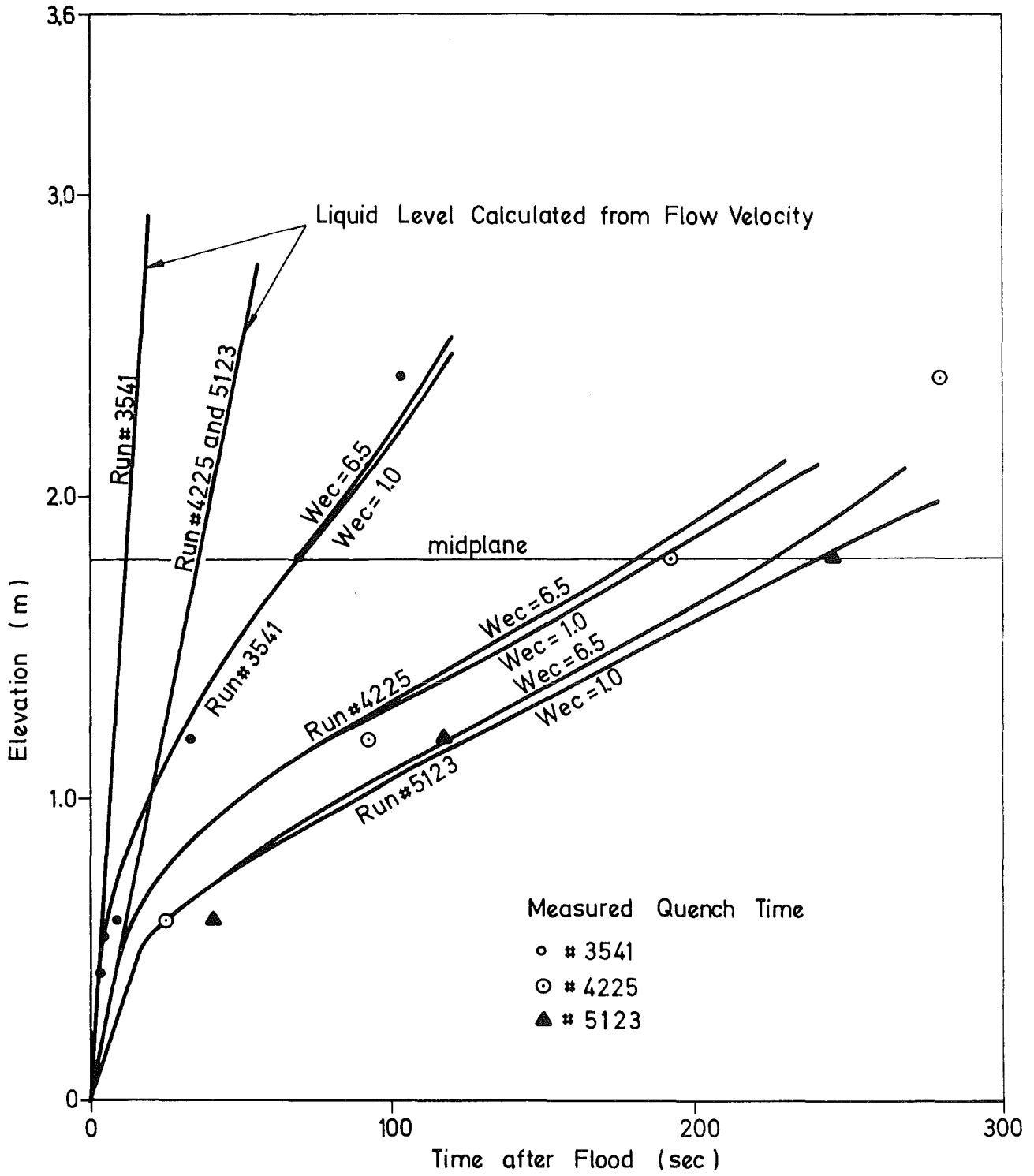


Fig. 5-4

Calculated Quench Position versus Time after Flood

Table 5.2

Comparison of Calculated Quench Temperatures with the Measured Temperatures

Run Number	3 5 4 1		4 2 2 5		5 1 2 3	
Elevation (feet)	Measured Temperature 5 F 6 G	Calculated Temperature 1)Wec = 6.5 2)Wec = 1.0	Measured Temperature 5 F 6 G	Calculated Temperature 1)Wec = 6.5 2)Wec = 1.0	Measured Temperature 5 F 6 G	Calculated Temperature 1)Wec = 6.5 2)Wec = 1.0
2	443.9 456.1	1)461.5 2)461.4	427.8 389.4	1)482.2 2)482.2	386.1 386.7	1)390.9 2)391.8
4	503.9 487.2	1)535.7 2)536.2	428.3 418.3	1)457.3 2)464.8	381.7 405.0	1)428.2 2)430.6
6	400.0 381.1	1)463.2 2)458.7	423.3 331.7	1)423.7 2)429.5	456.7 433.3	1)421.7 2)441.1
8	350.0 344.4	1)369.4 2)373.3	467.2 393.9		392.2 387.2	
10	- -		369.4 298.9		307.8 256.1	

unit = °C

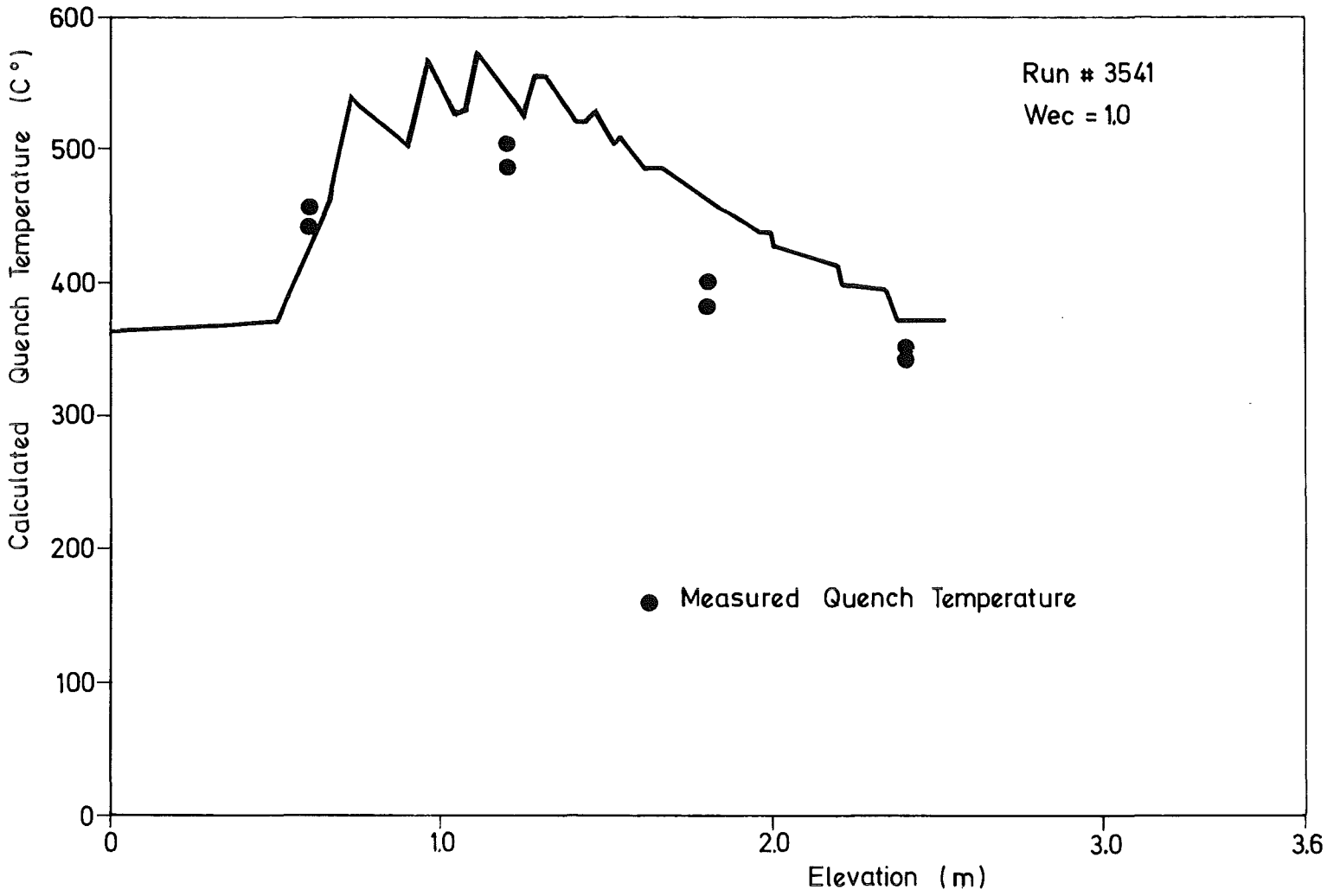


Fig. 5-5

Calculated Quench Temperature versus Elevation



## 6. CONCLUSION

Based on the flow pattern, shown in Fig. 2.5, and the quench model, and the subcooled film boiling correlation developed in Japan Atomic Energy Research Institute (JAERI), a reflood analysis code "REFLA-1D" was developed.

Comparing the calculated results and PWR-FLECHT data for three cases, the following conclusions were obtained:

- 1) The calculated overall temperature histories for critical Weber number  $We_c = 1.0$  agree considerably well with PWR-FLECHT's temperature histories.
- 2) In the transition flow region, the tendency of the temperature histories by calculation is different from the PWR-FLECHT's results. Hence further investigations on the transition flow region are necessary.
- 3) In earlier stage before turnaround time, the calculated temperature histories is different from the measured. For this point further investigations are necessary.
- 4) The calculated water droplet size is in the range measured by Schmidt for the critical Weber number  $We_c = 1.0$ .
- 5) The sensitivity of critical Weber number for the quench phenomenon is low but  $We_c = 1.0$  gives better results.
- 6) The calculated quench phenomena agreed with the quench phenomena of PWR-FLECHT except in earlier stage before turnaround time and for the rewetting type quench mode. The errors of quench time and quench temperature are in the range of  $\pm 16$  seconds and 100 to  $-25^{\circ}\text{C}$  respectively.

- 7) The calculation is relatively stable and the computing time is about the same as a real time for a IBM 370 computer.

ACKNOWLEDGEMENT

The author would like to thank Mr. S. Malang for his helpful advice and encouragement and several helpful discussions with the members of Institut für Reaktorbauelemente (IRB) are gratefully acknowledged.

The author was delegated from Japan Atomic Energy Research Institute (JAERI) for one year since July, 1975.

The author is indebted to Dr. M. Fischer, the head of Project Nuclear Safety (PNS) and Prof. Dr. U. Müller, the head of IRB for having the opportunity to study this problem in IRB.

References

- /1/ Murao Y., Sudoh T., Iguchi T., Sudo Y. and Yamazaki Y.  
Reflood Analysis Code "REFLA-1"  
presented at the conference of Japan Atomic Energy Society,  
Fukuoka (1974)
- /2/ Yamanouchi A.,  
Effect of core spray cooling in transient state after loss  
of coolant accident,  
J. Nucl. Sci. Techn. 5 (1968) 547
- /3/ Ellison M.E.,  
A Study of the Mechanism of Boiling Heat Transfer,  
Memo 20-88. Jet Propulsion Lab. (1958)
- /4/ Roache P.J. ,  
Computational Fluid Dynamics,  
Hermosa Publishers (1972)
- /5/ Murao Y. and Sudoh T.,  
A Study on the Quench Phenomena during Reflood Phase (1)  
to be published (JAERI-M-6984)
- /6/ Sudo Y. and Murao Y.  
Film Boiling Heat Transfer during Reflood, Process  
JAERI - M - 6848, (1976)
- /7/ Cadek F.F., Dominics D.P. and Leyse R.H., PWR-FLECHT  
Full Length Emergency Cooling Heat Transfer  
Final Report  
WCAP - 7665 (1971)
- /8/ Schmidt, H.  
Gesellschaft für Kernforschung  
Institut für Reaktorbauelemente  
Private Communication (1976)

- /9/ Groeneveld D.C.,  
The Thermal Behaviour of a Heated Surface at and beyond  
Dryout  
AECL - 4309 (1972)
- /10/ Blair J.M.  
An Analytical Solution to a Two-Dimensional Model of the  
Rewetting of a Hot Dry Rod  
Nucl. Eng. and Design 32 (1975) 159-170
- /11/ Thompson T.S.  
Rewetting of a Hot Surface  
5th Int. Heat Trans. Conf., Tokyo, (1974)
- /12/ Cermak J.O. et al.  
PWR Full Length Emergency Cooling Heat Transfer (FLECHT)  
Group 1 Test Report  
WCAP - 7435, (1970)
- /13/ Kattoh Y.  
Introduction to Heat Transfer (in Japanese)  
Yohkendo, (1965)
- /14/ Eckert E.R.G. and Drake R.M.,  
Analysis of Heat and Mass Transfer,  
Mc Graw-Hill Book Comp., (1972)
- /15/ Mac Farlane R.D.  
An Analytical Study of the Transient Boiling of Sodium  
in Reactor Coolant Channels  
ANL-7222, (1966)
- /16/ Kalinin E.K., Berlin I.I. and Kostynk V.V.  
Film-Boiling Heat Transfer  
Advances in Heat Transfer 11 (1975) 51-197,  
Academic Press, (1975)

- /17/ Bromley L.A.  
Heat Transfer in Stable Film Boiling  
Chem. Eng. Progr. 46, 221,(1950)
- /18/ Kalinin E.K. et al.,  
Investigation of Film Boiling in Tubes with Subcooled  
Nitrogen Flow,  
Proc. Int. Heat Transfer Conf., 4th, Paris,(1970)
- /19/ Ingebo R.D.  
Drag Coefficient for Droplets and Solid Spheres in  
Clouds Accelerating in Air-Streams,  
N.A.C.A. Techn. Note 3762 (1956)
- /20/ American Nuclear Society Standards  
Decay Emergency Release Rate Following  
Shut down of Uranium Fueled Reactors  
ANS-5 (1971)
- /21/ Murao Y. et al.  
Report on Reflood Series 1 Experiment  
(in Japanese)  
JAERI - M - 6551 (1976)

NOMENCLATURE

$c$	-	a factor for eq. (2.9)
$C^*$	-	Caurant number ( $\equiv U\Delta t/\Delta Z$ )
$C_D$	-	drag coefficient
$C_\ell$	m	wetting perimeter
$C_p$	kcal/kgK	specific heat
$D_d$	m	droplet diameter
$D_e$	m	equivalent diameter
$F$	-	friction coefficient defined by eq. (2.20)
$F_s$	-	shape factor defined by eq.(2.42)
$G$	kg/m <sup>3</sup>	mass velocity
$g$	m/h <sup>2</sup>	accelaration of gravity
$H$	kcal/kg	enthalpy
$H_{fg}$	kcal/kg	heat of exaporation
$h$	kcal/m <sup>2</sup> hK	heat transfer coefficient
$L$	m	linear dimension in eq. (2.26)
$L_{crit}$	m	critical wave length defined by eq. (2.25)
$Nu$	-	Nusselt number
$n$	1/m <sup>2</sup> h	number flux
$Pr$	-	Prandtl number
$p$	kg/m <sup>2</sup>	pressure
$Q$	kcal/m <sup>3</sup> h	heating power in unit volume
$\dot{Q}$	kg/m <sup>4</sup>	mass transferred from liquid phase to vapor phase in unit volume of two-phase mixture
$Re$	-	Reynolds number

S	$m^2$	cross section of flow channel
T	$^{\circ}C$	temperature
$T_o$	$^{\circ}C$	critical temperature like a Leidenfrost temperature
$T_R$	$^{\circ}C$	rewetting temperature
t	h	time
U	m/h	velocity
V	$m^3$	volume
We	-	Weber number defined by eq. (2.36)
We <sub>c</sub>	-	critical Weber number
x	-	quality
$X_{tt}$	-	Lockhart-Martinelli's parameter defined by eq. (3.5)
Z	m	elevation
$\alpha$	-	void fraction
$\beta$	-	ratio defined as $\beta \equiv \rho_L / \rho_g$
$\gamma$	-	ratio surface area to the area of flow channel wall
$\Delta U$	m/h	slip velocity
$\epsilon$	$kcal/m^2 h K^4$	Stefan Boltzmann Constant
$\lambda$	kcal/mhK	thermal conductivity
$\mu$	$kg h/m^2$	dynamic viscosity
$\nu$	$m^2/h$	kinetic viscosity
$\rho$	$kg h^2/m^4$	density
$\sigma$	kg/m	surface tension



$\tau$	$\text{kg/m}^2$	shearing stress
$\phi$	$\text{kcal/m}^2\text{h}$	heat flux
$\phi^2_L$		multiplication factor defined by eq. (2.22)

Indices

BOIL	boiling
C	coolant
crit	critical
CONV	convection
d	droplet
eff	effective
F	fuel
g	gas phase
L	liquid phase
L or g	liquid or gas phase
M	mean
MIN	minimum
MAX	maximum
q	quench
R	radiation
sat	saturated
sub	subcooled
t	total
w	wall (clad surface) (Two: temperature of the wall just before quenching)
VD	vapor to droplets
WV	wall to vapor